ACCELERATED OPTIMIZATION USING COHERENT ISING MACHINES

(コヒーレント・イジングマシンを用いた最適化問題の計算)

A DISSERTATION SUBMITTED TO
THE DEPARTMENT OF INFORMATION SCIENCE AND TECHNOLOGY
AND THE COMMITTEE ON GRADUATE STUDIES OF
THE UNIVERSITY OF TOKYO
IN PARTIAL FULFILLMENT OF THE REQUIREMENTS
FOR THE DEGREE OF
DOCTOR OF PHILOSOPHY

Kai Yan
顔　開

June 2013

Committee:

Masaru Kitsuregawa (Chair)

Jun Adachi

Yasuhiko Arakawa

Takashi Chikayama

Kenjiro Taura

Supervisor:

Yoshihisa Yamamoto

Thesis advisor | Author

Yoshihisa Yamamoto | **Kai Yan**

Accelerated optimization using coherent Ising machines

Abstract

Quantum computation takes advantage of quantum physics such as quantum parallelism and quantum interference, to perform calculations in an exponentially parallel way. Quantum computation realizes an exponential speed up over classical computers in solving problems such as factorization. However, the application is severely limited due to the computation model using unitary transformation, and to implement a scalable system remains a challenging task.

A new approach that benefits from a coherent quantum system to speed up the search of ground state of Ising model is proposed. The coherent Ising machine is based on one master laser and multiple mutually injection-locked slave lasers, where the master laser locks the optical frequency and phase of all slave lasers to keep the quantum coherence all over the system. The Ising model is implemented by coherent feedback network using optical interference circuits. The ground state of the Ising model corresponds to the polarization configuration with the minimal gain and loss, which emerges spontaneously through the natural mode competition induced by cross-gain saturation. The open dissipative system is more robust against noise thus make it more practical to be implemented. A NP-complete problem can be reduced as the Ising model, which provides the proposed system a wider range of applications

compared to the unitary transformation system.

In this thesis we introduce the coherent Ising machine using laser network. An efficient mapping of 3 Satisfiability problem (3SAT) to Ising model is proposed. The mapping method reduces a 3SAT problem with N variables to an Ising model with N spins, which can be implemented using a system with N slave lasers. We also propose a Binary search method to determine the optimal pumping power which provides the highest probability of finding the ground state in $O(logM)$ steps for a 3SAT problem with M clauses. Simulations using different sized $3SAT$ problems are investigated and from which we find the computation time scaling with input problem size is reduced to $O(N^3)$ with the optimal pumping rate.

Contents

List of Figures

List of Tables

Acknowledgments

(To be Updated) If Newton's law predicts life a destiny, I believe Schrödinger's equation made every flash an amazing grace, specially the one that the first time I went to Professor Yoshihisa Yamamoto's office. I should start by thanking Professor Yoshihisa Yamamoto to give me the oppotuinity to join his team, where under his supervision I learned so much not only in professional field, but also experience of the research career. He provided me with the best circumstances to focus on the research. His insight and inspiration and guidance was always an motivation encouraging me to progress.

I would like to thank my oral defense committee: Professor Masaru Kitsuregawa, Jun Adachi, Yasuhiko Arakawa, Takashi Chikayama and Kenjiro Taura. I thank them for their time and interest, and for the interesting and important questions they asked.

I thank Dr. Tim Byrnes, who embarked me for the quantum world and tought me the knowledge hand by hand. I had the outstanding opportunity to work with him and I could not have completed my thesis without his help. I also thank Dr. Shoko Utsunomiya who had the excellent pioneer work for the project. I thank Dr. Michael Fraser who is the most frequently seen people in the office, and always had passionate topics to chat, related to science or not. I thank Dr. Natsuko Ishida, who offered me a great help on guiding the procedures towards the doctral degree. I also thank other members in the lab, Dr. Kenichiro Kusudo, Kenta Takada in Japan and Dr. Alireza Marandi, Zhe Wang in Stanford who gave me valuable discussions and suggestions.

I also would like to express my thanks to administrative office staff in Yamamoto

group: Yukiko Sato, Yoko Shioda for their constant support, and Yurika Peterman, Rieko Sasaki for their kindness when I visited Stanford.

I thank the support of Tokyu foundation to offer me the financial support for two years, which let me focused on research and without any worries about food and basic life support. I also thank the joyful moments and great memories with the memebers of Tokyu family.

Last but most important, I thank my parents and my fiancee Qian for their unconditional love and support, and my host family Professor Sataro Yamauchi, Kazuko Yamauchi, Tetsufumi Yamauchi and Fumiko Terata for their constant love and care from far.

I thank the support of this research project by National Institute of Informatics, The Funding Program for World-Leading Innovating R&D on Science and Technology, DARPA, JST/SORST, The University of Tokyo, and the Special Coordination Funds for Promoting Science and Technology.

To my parents.

Chapter 1

Introduction

"The best way to predict the future is to invent it." (Alan Kay, 1971)

A computation is physical. While the advancement in computing power never stopped changing the landscapes of one's daily life, the basic principle lying under the binary mind remains the same except the evolution from beads mounted on an abacus' rod to electron charges hold in a transistor gate. The computation speed can not surpass the limitation of its physical implementation. Therefore, the quest for a novel computation scheme based on alternative physical entities has been investigated in the past decades. Among those a quantum computer is expected as a new window opening towards the fields where classical manner becomes incapable. In this thesis, we introduce and explore the possibilities of a new way to unleash the power of a quantum coherent system.

1.1 Quantum computation

A quantum computer [2] utilizes principles in quantum mechanics to speed up certain kind of computations over classical computer. The computation is performed by manipulating qubits by a sequence of unitary transformation gates and reading out the result by measurements with the higher probability of finding the correct answer. The quantum computer realizes large speed up compared to classical computation in solving certain computationally intractable problems, by using algorithms such as Grover's random search [3] and Shor's factoring [4]. However, the quantum computer is difficult to implement due to the problem of scalability and decoherence, moreover, the difficulty of applying the unitary transformations to a wider field of practical problems such as optimization problems strictly limited the application of a quantum computer.

In the real world, one will frequently encounter optimization problems in the fields such as scheduling, circuit verification, chemical simulation and so on. An optimization problem aims to find a solution in the feasible region with the minimum or the maximum value of the objective function. The feasible region is the set of all possible solutions of the optimization problem, and the objective function associated with the problem determines how good a specific solution is. Optimization problems in NP-complete class [5] has a wide range of applications. Given a solution to a NP-complete problem the correctness can be quickly verified in polynomial time, whereas to find the candidate solution is computationally intractable due to an exponential growing in computational time with the increase of problem size. Members in NP-complete class can be transformed into each other in polynomial time complexity,

thus a fast algorithm or device that is effective to any specific form of NP-complete problem can benefit the whole class.

Given a NP-complete problem, one can transform it to a specific form in which it is easier solved using a specific kind of an algorithm or a physical computational device. In this thesis our interest is focused upon the Ising model which provides a mathematical prototype for studying various magnetic orders in frustrated spin lattice and random spin glasses [6] [7]. It is known that a NP-complete problem can be formulated as a ground state search problem of an Ising model [8], an Ising machine that can find the ground state spin configuration efficiently has been extensively searched in both classical and quantum domains [9]. The simulated annealing algorithm mimics the thermal annealing procedure in metallurgy [10]. Quantum adiabatic computation solves the Ising model by utilizing quantum mechanical tunneling across a potential energy landscape [11] [12] [13] [14] [15], which is shown to have superior performance over simulated annealing. As a variant of quantum annealing, quantum adiabatic computation was devised according to the quantum adiabatic theorem , whose power is proven to be equivalent to that of a quantum computer .

In the experimental realizations, the quantum annealing is implemented with either a sample of real magnetic crystal [16] [17] or molecular NMR technique [18]. In order to map a given mathematical problem onto such a quantum annealing Ising machine, nonlocal interaction J_{ij} must be implemented artificially irrespective of actual distance between two sites. This is extremely hard to achieve in real crystals or molecules. An Ising machine that harnesses the effect of Bose-Einstein condensation (BEC) and measurement-feedback control has been proposed in [19]. The machine

utilizes the bosonic final state stimulation property of BEC to attain the speedup in cooling down to the ground state by a factor of bosonic particle number per site [20]. However, a measurement feedback circuit which is required to implement nonlocal interactions J_{ij} is an inherently incoherent device and cannot create the quantum coherence between different sites. The cost resulting from this fact is that the computational time scales exponentially as a problem size of N [20]. So far as is known, no efficient algorithm exists for NP-complete problems.

A new Ising machine based on one master laser and N mutually injection-locked slave lasers is proposed in [21]. An Ising model is implemented by coherent feedback network using optical interference circuits instead of incoherent electrical measurement-feedback circuits. A spin degree of freedom σ_i at each site is represented by right or left circular polarization states of each slave laser. The ground state of an implemented Ising model which is represented with polarization configuration of N slave lasers emerges spontaneously through the natural mode competition induced by cross-gain saturation among all candidate polarization configurations. The objective function corresponds to the overall photon decay rate in the proposed system. The injection-locked laser system oscillates with a specific polarization configuration which minimizes the objective function (photon decay rate). A semiconductor laser is particularly attractive for this application because of its rapid intraband spin relaxation, small saturation power, short photon lifetime and compact size. A rapid spin relaxation process realizes equally populated conduction electron spins and valence hole spins, so that the particular polarization configuration with a minimum photon decay rate can oscillate alone by suppressing the oscillation of all the other

2^N polarization configurations. A saturation photon number N_s (or inverse fractional spontaneous emission coupling efficiency $\beta = 1/N_s$) of a semiconductor laser is many orders of magnitude smaller than that of the other types of laser systems. Therefore, the above cross-gain saturation can be switched on by an extremely small injection power. A photon lifetime of typical semiconductor lasers is 1psec, which allows a very large injection-locking bandwidth even with a very small injection power. A stable and fast operation of this computing machine originates from this fact that an injection locking bandwidth is extremely broad. Finally a large number of arrayed vertical cavity surface emitting semiconductor lasers (VCSEL) can be integrated into one chip. It is even possible to integrate hybridly those VCSELs with a master laser, other linear optical circuits and detectors, which makes a whole computing system very compact even for a large-scale Ising problem.

From the investigations so far, the proposed coherent Ising machine achieves a several magnitude of speed up over classical computers in solving several NP-hard problems [22]. A practical working machine have to repeat the computation process to find a good solution for a NP-hard problem. In this thesis we concentrate on the application of the system to NP-complete problems. The basic architectures for the coherent Ising machines is explained in detail, and the benchmark results for solving NP-complete problems using the machines is given and discussed.

1.2 Structure of the thesis

This thesis is structured in seven chapters as following:

Chapter 1: Introduction

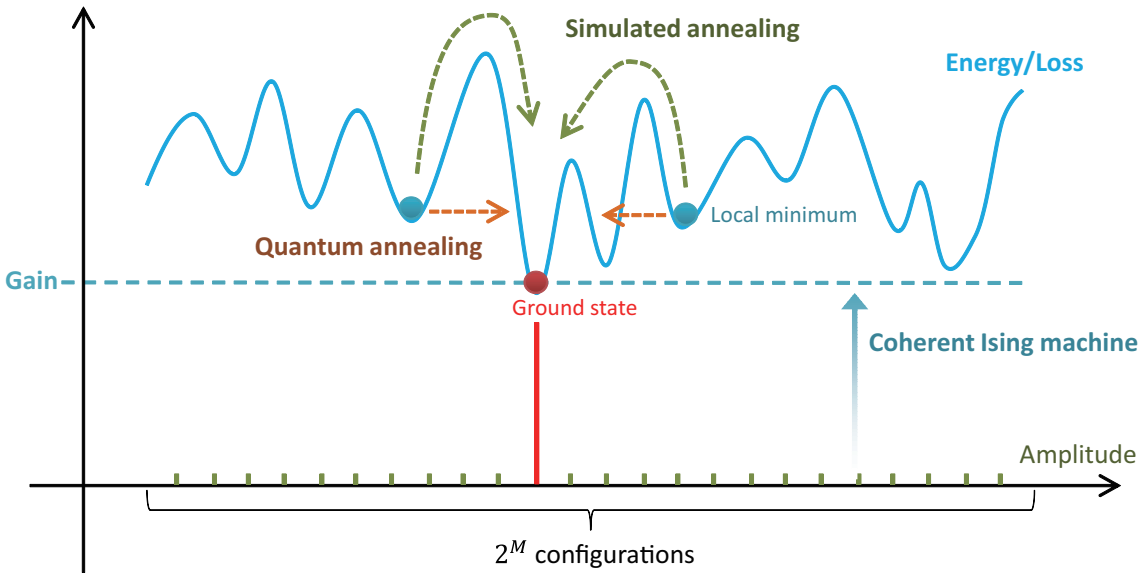

Figure 1.1: The concept picture of simulated annealing, quantum annealing and coherent Ising machine.

Chapter 2: Optimization Problems

Combinatorial optimization problems, including the definition of NP-hard class, NP-complete class and Ising model is explained and we review the transformation process for 3SAT problems into Ising model following the traditional method, meanwhile in contrast we present a more simple and efficient way to implement.

Chapter 3: Coherent Ising machines

A coherent Ising machine using injection-locked laser network is introduced with simulation results on finding the ground state of a given Ising model.

Chapter 4: Solving NP-complete problems

We will be going through a series of extension techniques to improve the computational performance in solving 3SAT problems. Extension schemes using optimal pumping determination and dynamic weighted clauses is added with simulation results showing the improvement. Benchmark results for 3SAT problems is given and

we discuss the advantages and difficulties of the system in practical use.

Chapter 5: Conclusion

We review the results and discuss our conclusions.

Chapter 2

Optimization Problems

2.1 Computational complexity

When people is proposed the most classical sentence of mankind: `i love you`, the response would be emotional. In contrast, for most case we encounter in the daily life has a deterministic answer. For example, to calculate the total price of a shopping list, to sort a list of names in alphabetic order, or to plan a trip around as more places as possible while save the expense to the minimum. These kind of problems can be solved using a computer, thus is called computational problems. The method and procedure to solve the problem using a computer is described as an Algorithm. The algorithm can be widely varied from a hand-calculation using fingers to an atmosphere simulation using a supercomputer. To evaluate the efficiency of an algorithm independent of any specific kind of hardware it is using, the Turing machine an abstract model of computation is introduced (Figure 2.1).

A Turing machine is a conceptual device that operates on a tape step by step

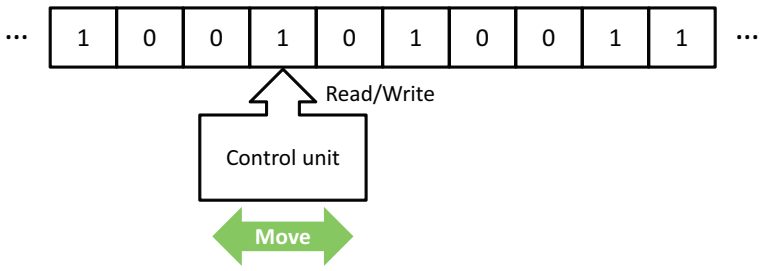

Figure 2.1: A schematic drawing of Turning machine

following a series of instructions. A deterministic Turing machine whose movement is completely determined by the current state and input, on the other hand, there is another type of the machine called Non-deterministic Turning machine . The Nondeterministic Turing machine works quite similar like a deterministic machine, however, given the same input it can have several alternative path to proceed . When it comes to an branch point, the machine is given the talent of choosing the correct one among all the possible successor states. In practical, to make a Nondeterministic Turing machine it actually has to simulate all possible paths simultaneously and selects the best one among the results.

The algorithm is depicted as the instructions, and its computational complexity is evaluated by the number of steps and length of the tape it consumes on a Turing machine. In the theoretical research, the exact number of the steps is not important, on the other hand, the asymptotic time complexity with the growth of problem size N is studied.

The big-O notation is employed such that $T(M) = O(f(M))$, where $f(M)$ is also a function of M, meaning that there exist a sufficient large M_0 and a number ϵ such that $|T(M)| \leq \epsilon f(M), if M > M_0$ [23]. Which means that $T(M)$ grows no

faster than $f(M)$ asymptotically. On the contrary, another big-Ω notation, namely $T(M) = \Omega(f(M))$, is defined if $T(M)$ grows faster than $f(M)$ asymptotically. It means that there exist a sufficient large M_0 and a positive number ϵ such that $|T(M)| \geq \epsilon f(M), if M > M_0$.

With the notation, we are able to classify computational problems into two categories. The easy problems are generally referred to those that can be solved with polynomial time complexity, namely $T(M)$ is a polynomial function. The set of such easy problems are denoted by class P. On the other hand, the problems to which solutions with polynomial time complexity are not yet found are difficult problems. For example, if the best solution to a problem is exponential, i.e., $T(M) = O(2^M)$, the required time to solve the problem will quickly become much longer than that for solving a P problem.

2.2 NP-complete class

People have defined a special subset of problems called NP-problems, which can be solved by the Non-deterministic Turing machine in polynomial time. As the deterministic Turing machine is a special case of non-deterministic Turing machines and is the current theoretical model of computers, P problems are also a subset of NP-problems, namely P $\subset$ NP. However, the opposite way, i.e. NP $\subset$ P remains one of the most important open question in computer science. Beside NP-problems, a superset of NP-problems is called NP-hard problems, which contains problems even difficult than NP problems. To address the question whether P = NP, the concept of NP-complete problems has been proposed [24] [25] [26]. An NP-complete problem is

an NP problem whose solution in polynomial time will immediately lead to the solutions in polynomial time to all NP-problems. Therefore, if a solution in polynomial time is found to one of the NP-complete problems, we subsequently prove P = NP, and solving an NP-complete problem in polynomial time has raised substantial interests in the community. Figure 2.2 illustrate the classification of all computational problems for different answers.

The proof of a problem to be an NP-complete problem is achieved by establishing the mapping in polynomial time to another NP-complete problem. So far people have discovered and proved that many important problems are unfortunately NPcomplete. For example, satisfiability(SAT) is the first known NP-complete problem [24]. In addition, Hamiltonian path problem, traveling salesman problem(TSP), subset sum problem, graph coloring problem, etc, are all proved to be NP-complete [25]. These problems have wide applications in many scientific and engineering fields, and thus the computational difficulty generated by the exponential time complexity from current best algorithms becomes a critical bottleneck in those fields.

An optimization problem aims to find a solution in the feasible region with the minimum or maximum value of the objective function. The feasible region is the set of all possible solutions of the optimization problem, and the objective function associated with the problem determines how good a specific solution is. Generally such a problem can be formulated as a computational problem to find the particular combination of N variables v_1, v_2, $...v_M$ which minimizing a cost function $E(v_1, v_2, ...v_N)$. For example, a traveling salesman problem [5] is to find a path through a weighted graph which starts and ends at the same vertex, including every other vertex exactly

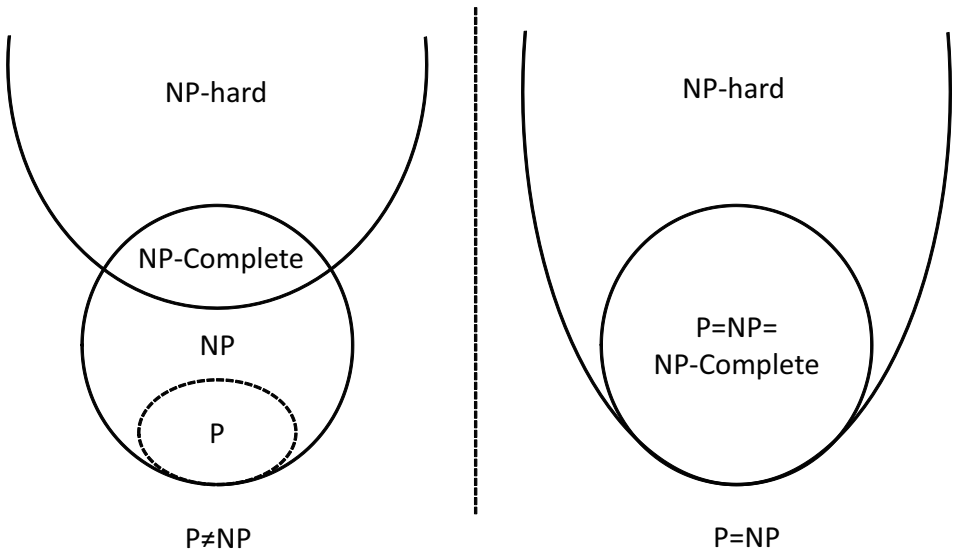

Figure 2.2: Complexity class

once, and simultaneously minimizes the total cost of edges.

For each optimization problem, there is a corresponding decision problem that asks whether there is a feasible solution with a particular characteristic, while the optimization problem asks what is the best solution. For example, the traveling salesman problem is an optimization problem, while the corresponding decision problem asks if there is a Hamiltonian cycle with a cost less than a given specific amount k [5].

An optimization problem belongs to class NP (Nondeterministic Polynomial) can be solved in polynomial time only by a nondeterministic machines. A nondeterministic machine cannot be simulated by a deterministic Turing machine without an exponential growth of computational time. Among NP problems, there are certain subsets of problems known as NP-complete problems [5]. A problem belonging to this class has two properties. The first is given a solution to the problem, it can be verified for correctness in polynomial time. The second is that a specific NP-complete problem

can be transformed into another NP-complete problem in polynomial time. Therefore if any specific NP-problem can be solved in polynomial time, so can every problems in the class. NP-complete problems are considered to be computationally intractable even for a moderate problem size, since there is no known fast algorithm to find a candidate solution that runs in deterministic Turing machine with polynomial steps. Solving NP-complete problems have a high degree of practical importance since many optimization problems one frequently encounters belongs to the NP-complete class, such as the SATISFIABILITY Problem (SAT), Graph Partition Problem (GPP) or MAX-CUT problem.

2.3 Ising model

An Ising model [27] provides a prototype framework for studying various magnetic orders in frustrated spin lattice and random spin glasses. An electronic spin has a freedom degree similar to kinetic rotation, namely, spin angular momentum. In the Ising model, a spin σ_i is quantumized in one direction (projection along z-axis) whose value can be either $+1$ (Up) or -1 (Down). A spin is coupled with other spins, namely σ_j, and the interaction between two coupled spins contributes an amount of energy equivalent to $J_{ij}\sigma_i\sigma_j$ to the total energy H (the Hamiltonian) of the system. When $J_{ij} < 0$ it is called ferromagnetic interaction, in which two spins taking the identical value will have lower energy (stable) and generate a stronger magnetic field. On the contrary, if $J_{ij} > 0$ it is called antiferromagnetic interaction, since two spins taking opposite value will have lower energy and generate a weaker magnetic field. In the spin lattice, only the coupling of nearest neighbors is considered. However, as we will

see in the following chapters, to solve a NP-complete problem using Ising model it is required to generate couplings between two arbitrary spins, which is realized by artificial optical interactions in the proposed system. In the Ising model, the energy of each spin is also induced on the external magnetic field where the spin is placed, namely $\lambda_i \sigma_i$, where λ_i express the magnitude of induced energy for spin σ_i. Therefore, for a system with N spins, the energy of the system is given by the Ising Hamiltonian

$$H = \sum_{i<j} J_{ij} \sigma_i \sigma_j + \sum_i \lambda_i \sigma_i. \tag{2.1}$$

It is known that a NP-complete problem can be easily formulated as a ground state search problem of an Ising spin model [28]. For example, given the graph shown in Figure 2.3 which has several vertices and edges who is given a certain amount of weight. The goal is to find a way of dividing the vertices into two groups with equal number, while the total weight of edges come across the boundary achieves the minimal value. We label each vertex with an index σ_i and the edge between vertex σ_i and σ_j as J_{ij}. If we assign the vertices who should be resided in group A with $+1$ and those in the other group B with -1, with this construction the question now becomes to find a specific spin configuration which makes the ground state of (2.1) without the Zeeman terms.

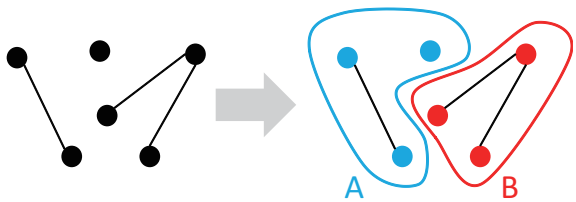

Figure 2.3: A simple MAX-CUT problem

In later chapters we will see that the proposed coherent system takes Ising model

as a starting point of encoding optimization problems and solve them by finding the ground state of the Ising model with advantages arisen from quantum systems. The transformation between NP-complete problems provides a wider application for the system. Therefore given a problem it has to be transformed into Ising model in the first step. The efficiency of the mapping method can be different for various ways. In this chapter we show a transformation procedure from several representative NP-complete problems into Ising model in detail and analyze the efficiency.

2.3.1 3SAT problem to Ising model

In this section we present the transformation procedure from 3SAT problem to Simple MAX-CUT problem. The 3SAT is one of the representative NP-complete class problems which is usually taken as a root from which varied problems are given the proof to be NP-complete. It also has a wide range of correspondence to practical encounters such as circuit design and verification. The Simple MAX-CUT problem is directly correspondent to an Ising model with all the edges to have equal unit weight. Therefore following the transformation one can quickly encode a large number of NP-complete problems into Ising model and solve it using an Ising machine.

Following the way given in [1], there are two steps including 3SAT to MAX-2-SAT, and then MAX-2-SAT to Simple-MAX-CUT. Firstly we formulate the first two problems respectively as

Definition of 3SAT

INSTANCE: Disjunctive clauses C_1, C_2, ..., C_m, each containing exactly three literals. Each literal represents a boolean variable or its negation

$$S = \bigcup_{i=1}^{M} (A_i + B_i + B_i), A_i, B_i, C_i \in \bigcup_{j=1}^{N} \{X_j, \bar{X}_j\}. \tag{2.2}$$

QUESTION: Is there a truth assignment to the variables which satisfies all the clauses?

Definition of MAX-2-SAT

INSTANCE: Disjunctive clauses C_1, C_2, ..., C_p, each containing at most two literals, positive integer K.

QUESTION: Is there a truth assignment to the variables which satisfies K or more clauses?

Given the 3SAT problem, we label them $(a_1 + b_1 + c_1)$ through $(a_m + b_m + c_m)$, the corresponding set S' of clauses and value K for MAX-2-SAT are given by:

$$\begin{aligned} S' = \bigcup_{i=1}^{M} \{&(A_i), (B_i), (C_i), (D_i), (\bar{A}_i + \bar{B}_i), (\bar{B}_i + \bar{C}_i), (\bar{B}_i + \bar{C}_i), \\ &(A_i + \bar{D}_i), (B_i + \bar{D}_i), (C_i + \bar{D}_i)\}, \\ &K = 7M. \end{aligned} \tag{2.3}$$

Here $7M$ or more of the clauses in S' can be satisfied simultaneously if and only if the original set S is satisfiable. If we have any satisfying assignment for S, then either one, two, or three of A_i, B_i, C_i must be set "true" for each i. In all three cases, there is a truth setting for D_i causing precisely seven of the clauses in S' arising from clause i to be satisfied. No setting of D_i will permit more than seven of the ten clauses to be satisfied, and at most six of the clauses can be satisfied if all of A_i, B_i, and C_i are "false".

For example we are given a simple 3SAT problem as $(A+B+C)$, the correspondent MAX-2-SAT clauses is given by:

$$(A)(B)(C)(D)(\bar{A}+\bar{B})(\bar{A}+\bar{C})(\bar{B}+\bar{C})(A+\bar{D})(B+\bar{D})(C+\bar{D}) \tag{2.4}$$

with the satisfying condition $K \geq 7$. One can verify the above statements by taking all three variables $A, B, C = FALSE$ so that no matter how we change the value of variable D there can not be more than 6 satisfied clauses in (2.4). On the other hand, with more than 1 variable among A, B, C that is assigned to be $TRUE$ will make at least 7 satisfied clauses in (2.4) independent of what assignment the variable D takes.

Next we transform the MAX-2-SAT to Simple MAX-CUT which is defined as:

Simple MAX-CUT

INSTANCE: Graph $G = (V, E)$, weight function $w(e) = 1$ for each edge $e \in E$, positive integer W.

QUESTION: Can the set V of vertices be partitioned into two disjoint sets V_1 and V_2 such that the sum of the weights of the edges from E that have one endpoint in each set is at least W?

Let clauses C_1, C_2, ..., C_p, and integer K be given as input for the MAX-2-SAT problem. Each clause of the MAX-2-SAT problem has exactly two literals, we label them as (A_1+B_1), (A_2+B_2), ..., (A_p+B_p). Assume that no two clauses are identical.

We create a graph corresponding to the given input MAX-2-SAT problem in two steps. Firstly construct the vertices and a basic framework of edges, and then adding in some edges which represents the given problem. Let X_1, X_2, ..., X_n, be the variables

occurring (either complemented or uncomplemented) in the p clauses. The set V of vertices for the graph G is

$$\begin{aligned} V = \quad & \{T_i : 0 \leq i \leq 3p\} \cup \{F_i : 0 \leq i \leq 3p\} \cup \{t_{ij} : 1 \leq i \leq n, 0 \leq j \leq 3p\} \\ & \cup \{f_{ij} : 1 \leq i \leq n, 0 \leq j \leq 3p\} \cup \{x_i : 1 \leq i \leq n\} \cup \{\bar{x}_i : 1 \leq i \leq n\}. \end{aligned} \tag{2.5}$$

The basic framework E_1 of edges is

$$\begin{aligned} E_1 = \quad & \{\{T_i, F_j\} : 0 \leq i \leq 3p, 0 \leq j \leq 3p\} \cup \{\{t_{ij}, f_{ij}\} : 1 \leq i \leq n, 0 \leq j \leq 3p\} \\ & \cup \{\{x_i, f_{ij}\} : 1 \leq i \leq n, 0 \leq j \leq 3p\} \cup \{\{\bar{x}_i, t_{ij}\} : 1 \leq i \leq n, 1 \leq j \leq 3p\} \end{aligned} \tag{2.6}$$

For any given partition $V = V_1 \cup V_2, V_1 \cap V_2 = \emptyset$, edge $\{u, v\}$ is bad if both u and v belong to the same set in the partition and is good otherwise. All edges in E_1 will be good for any partition $V = V_1 \cup V_2$ which obeys (a)all T_i belong to the same set in the partition and all F_i belong to the other set, and (b)for each i, x_i and all t_{ij} belong to the same set in the partition and $\bar{x}_i$ and all f_{ij} belong to the other set. If any pair F_i, F_j belong to different sets in the partition, then at least $3p + 1$ edges from E_1 will be bad, since each such pair of nodes are mutually adjacent to $3p + 1$ other nodes. Similarly, if any pair x_i, $\bar{x}_i$ belong to the same set in the partition, then at least $3p + 1$ edges from E_1 will be bad, since there are $3p + 1$ disjoint 3-edge paths between x_i and $\bar{x}_i$.

The following additional edges are included in G to represent the problem specific information:

$$\begin{aligned} E_2 = \quad & \{\{a_i, b_i\} : 1 \leq i \leq p, \ \textit{and } a_i \neq b_i\} \\ & \cup \{\{a_i, F_{2i-1}\} : 1 \leq i \leq p\} \cup \{\{b_i, F_{2i}\} : 1 \leq i \leq p\}. \end{aligned} \tag{2.7}$$

The input for Simple-MAX-SAT is the graph $G = (V, E_1 \cup E_2)$ and $W = \mid E_1 \mid + 2K$.

Given a truth assignment for the n variables which satisfies K or more clauses, construct the partition $V = V_1 \cup V_2$ as follows:

$$\begin{aligned} V_1 = \ & \{F_i : 0 \leq i \leq 3p\} \cup \{x_i : x_i = false, 1 \leq i \leq n\} \\ & \cup \{t_{ij} : x_i = false, 1 \leq i \leq n, 0 \leq j \leq 3p\} \\ & \cup \{\bar{x}_i : x_i = true, 1 \leq i \leq n\} \\ & \cup \{f_{ij} : x_i = true, 1 \leq i \leq n, 0 \leq j \leq 3p\}. \end{aligned} \tag{2.8}$$

$$V_2 = V - V_1. \tag{2.9}$$

For each satisfied clause, one or both of a_i and b_i belong to V_2, exactly two edge in E_2 arising from that clause must be good, and every edge in E_1 is good. Thus we have at least $W = \mid E_1 \mid + 2K$ good edges.

Given a partition $V = V_1 \cup V_2$ for which W or more edges are good. Since $K > 0$ and $\mid E_2 \mid \leq 3p$, the number of bad edges cannot exceed $3p$. This implies that all the F_i must belong to the same set, say V_1. For the same reason, exactly one of each pair x_i, $\bar{x}_i$ must belong to V_1. Thus, a consistent truth assignment is obtained by setting x_i "true" if and only if x_i belongs to V_2. For this truth assignment, clause i is satisfied whenever a_i or b_i or both belong to V_2. However, among the edges in V_2 arising from clause i, exactly two are good if one or both of a_i and b_i belong to V_2 and none are good if a_i and b_i both belong to V_1. Therefore, since at least $2K$ edges from V_2 must be good, this truth assignment must satisfy at least K clauses.

As an illustrative example, the graph generated for a clause such as $(A + B)$ is given in Figure 2.4.

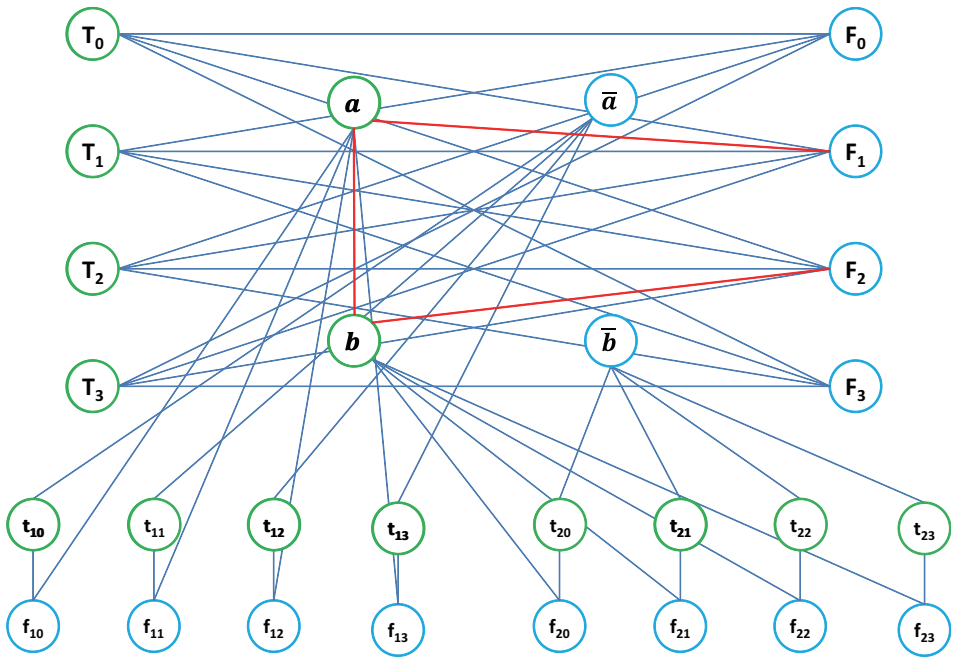

Figure 2.4: The Simple MAX-CUT graph correspondent to a single clause $(A + B)$ generated using method in [1]. The optimal separation satisfying the clause is given by grouping the vertices with identical color. The problem specific edges are emphasized by red.

Although a physical device that implements the Simple MAX-CUT graph only need to either connect or disconnect each pair of vertices, the cost in implementing the vertices of required number can be huge. For a 3SAT problem with N variables and M clauses, the number of variables is increased to $N+M$ in the first stage as the auxiliary variable D_i is introduced into every clause. In the second stage from (**??**) we see the number of vertices required is $(2+80M)(N+10M)+40M$. For a realistic problem it requires a giant scale of graph which may not be practical to implement.

In MAX-CUT where we allow the weight function to take integers, i.e. $w(e) \in Z^+$ for each edge $e \in E$, the edges connected between the same pair of vertices in (**??**) can be combined as one associated with the weight of number of the edges. Therefore the

required number of vertices for the graph can be greatly slimed to $2(N+M+1)+2$. The MAX-CUT graph for the clause $(A+B)(\bar{A}+\bar{B})$ is shown in Figure 2.5 for a comparison.

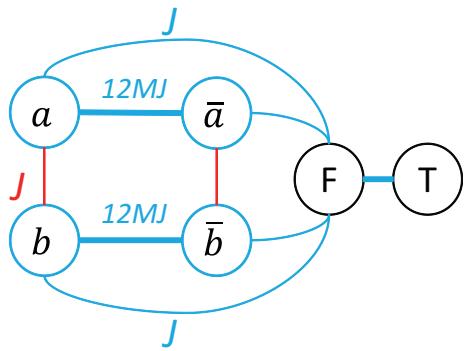

Figure 2.5: The MAX-CUT graph for $(A+B)(\bar{A}+\bar{B})$. Problem specific edges are colored in red.

To map a MAX-CUT problem onto an Ising model, a cost function is defined as

$$H_{MC} = \sum_{i<j} J_{ij}(1-\sigma_i\sigma_j)/2 \tag{2.10}$$

where $J_{ij} = w(e) \in Z^+$ if the points are connected by $e \in E$ and 0 otherwise. We slightly change (2.10) to

$$H'_{MC} = \sum_{i<j} J'_{ij}(1-\sigma_i\sigma_j)/2, \ where \ J'_{ij} = 1 - \frac{J_{ij}}{|J_{MAX}|} \tag{2.11}$$

where J_{MAX} is the biggest one among all the given $J_{ij} = w(e) \in Z^+$. By (2.11) the J'_{ij} is normalized to $[0,1]$. The problem is then to find the σ_i configuration that minimizes (2.11) and verify if

$$\sum_{k=0}^{N_k} J'_k \leq N_k - \frac{K}{J_{MAX}}, \tag{2.12}$$

where J'_k represents the J'_{ij}s in (2.11), which are the weights of the edges that have one endpoint in each set, N_k is the total number of J'_ks. We can drop first term and

constant factors in front of the summation of (2.11), which gives

$$H_I = \sum_{i<j} J'_{ij}\sigma_i\sigma_j. \tag{2.13}$$

2.3.2 3SAT problem to Ising model with 3 spin interaction

The Garey's method provides a proven way of transforming 3SAT problem to an Ising model. Although the number of sites required remains in polynomial growth order, even for a simple 3SAT problem it can be a graph containing a huge number of sites. As we will see in the later chapters, each site in the Ising model is represented as a laser site. An inefficient transformation which requires a huge number of sites brings unnecessarily a difficulty into the physical implementation.

In this section, we present a simpler but much more efficient approach to map a 3SAT problem into an Ising model. The method only requires N sites for a 3SAT problem with N variables, and the number of clause M can be eliminated from the scaling factor. The method request a 3 spin coupling term into the Ising Hamiltonian, however, it can be practically eliminated or virtually implemented using an artificial way in the physical implementation.

We start illustrating the presented method by giving a 3SAT problem with a collection S of M clauses, each clause $C \in S$ has exactly 3 literals

$$\begin{aligned} C_i &= A_i \cup B_i \cup C_i, \\ S &= \bigcap_{i=1}^{M} C_i, \end{aligned} \tag{2.14}$$

where A_i, B_i and C_i is either a variable X_i or its negation $\bar{X}_i$ and the 3SAT problem asks if there exists any satisfying truth assignment for S. By De Morgan's law we

flip (2.14) into

$$\bar{C}_i = \bar{A}_i \cap \bar{B}_i \cap \bar{C}_i,$$
$$\bar{S} = \bigcup_{i=1}^{M} \bar{C}_i, \tag{2.15}$$

our aim then is to assign the logical variables X_i to make $\bar{S}$ equals to logical $FALSE$. The mapping is to convert a logical statement with either $TRUE$ or $FALSE$ into an algebraic expression where a spin takes value of ± 1, therefore we make a correspondent Hamiltonian to each clause C_i such as

$$H_{Ci} = -\frac{1}{8}(1 + s_{ai}a_i)(1 + s_{bi}b_i)(1 + s_{ci}c_i), s_{ai}, s_{bi}, s_{ci}, a_i, b_i, c_i \in \{\pm 1\}, \tag{2.16}$$

where $s_{ai} = 1$ for A_i or $s_{ai} = -1$ for $\bar{A}_i$, and accordingly s_{bi} and s_{ci} are decided. The a_i, b_i and c_i are Ising spins correspondent to the logical variable A_i, B_i and C_i respectively, by matching the spin $+1$ with the logical $TRUE$ and -1 with $FALSE$, we have $H_{Ci} = -1$ if $C_i = TRUE$ and $H_{Ci} = 0$ if $C_i = FALSE$. To satisfy all the M clauses for S in (2.15), a summation is made by

$$H_S = -\frac{1}{8}\sum_{i=1}^{M}(1 + s_{ai}a_i)(1 + s_{bi}b_i)(1 + s_{ci}c_i). \tag{2.17}$$

By expanding (2.17) and eliminating the constant terms we have the Ising Hamiltonian

$$H = -\sum_{i=1}^{M} s_{ai}a_i + s_{bi}b_i + s_{ci}c_i - s_{ai}a_i s_{bi}b_i - s_{ai}a_i s_{ci}c_i - s_{bi}b_i s_{ci}c_i + s_{ai}a_i s_{bi}b_i s_{ci}c_i \tag{2.18}$$

Now the satisfying condition for S in (2.14) is made by if and only if $H = -M$. Giving an example of $(A+B+C)$ whose equal Ising model is $H = a+b+c-ab-ac-bc+abc$, the energy difference between $TRUE$ and $FALSE$ assignments can be quickly verified in Table 2.1.

a	b	c	H	H'
1	1	1	-1	0
1	1	-1	-1	-2
1	-1	1	-1	-2
1	-1	-1	-1	0
-1	1	1	-1	-2
-1	1	-1	-1	0
-1	-1	1	-1	0
-1	-1	-1	7	6

Table 2.1: Energy landscape

Notice here that if we simply drop the abc term in the Hamiltonian (2.18), the energy landscape is partly modified as shown by H' in Table 2.1. However, in this simple example the energy gap between satisfiable assignments and UNsatisfiable assignment still remains. As the problem becomes larger and complexed, the energy gap may not be retained and the energy of satisfiable solution and UNsatisfiable solution may collapse into each other. In Figure 2.6 we show a typical case for a sample problem with 5 variables and 15 clauses. As we see from the graph, where the number of UNsatisfied equals to 0 suggests a satisfying assignment, the ground state in the approximated Hamiltonian H' may not correspondent to that. The disappearance of abs term in (2.18) may lead to a satisfying solution into excited states.

Figure 2.6: Energy landscape for a 3SAT problem with 5 variables and 15 clauses. Ensemble result of 100 trajectories. The problem used is $(\bar{X}_5 + X_3 + \bar{X}_4)(\bar{X}_5 + X_3 + X_1)(\bar{X}_1 + X_5 + \bar{X}_4)(\bar{X}_3 + X_2 + \bar{X}_1)(X_2 + X_4 + X_3)(\bar{X}_4 + X_3 + X_2)(\bar{X}_1 + X_3 + \bar{X}_4)(\bar{X}_2 + X_1 + \bar{X}_5)(X_1 + X_2 + \bar{X}_4)(X_1 + X_5 + \bar{X}_2)(\bar{X}_3 + X_5 + X_1)(X_3 + X_4 + X_1)(\bar{X}_5 + \bar{X}_2 + \bar{X}_3)(\bar{X}_2 + \bar{X}_1 + \bar{X}_5)(X_2 + X_5 + X_3)$

Chapter 3

Coherent Ising machines

In this chapter we present the detailed design and working principles of the proposed Ising machine. We start by building up the basic of Lasers, and following the basic motion of a injection-locked laser system we explain how an Ising model is mapped.

3.1 Lasers

We start from the most basic type of laser to describe its working mechanism. The diagram of a typical single-mode laser is shown in Figure 3.1, which includes a gain medium, a pump source or excitation medium, an optical cavity and output coupler. The gain medium implements both linear amplification via stimulated and spontaneous emissions, and nonlinear saturation mechanisms via atomic absorption. The pumping can be generated by a power source or another incident laser. The cavity with two mirrors only allows certain oscillation frequencies and modes for the

internal field. The internal field $\hat{A}(t)$ of the cavity is built up by the competition

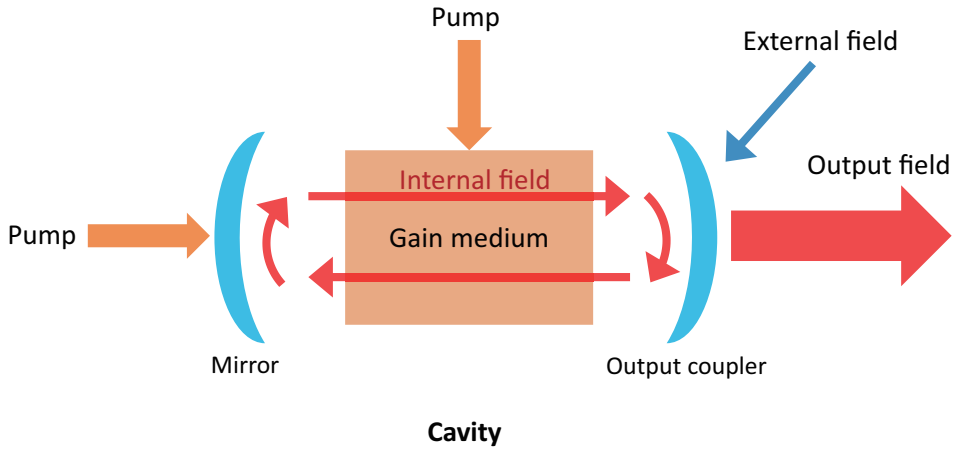

Figure 3.1: A schematic drawing of a typical laser.

between the gain and the loss. The field is amplified by the gain medium when it travels back and forth between the two mirrors. The generated photons either decay through the cavity loss or is absorbed by the gain medium. The gain and the loss compete against each other. Initially the gain is greater than the loss and the internal field builds up exponentially. After the field amplitude increases substantially, the nonlinear absorption becomes significant and eventually saturates the gain at steady state. The internal field decays via cavity loss, and the lost photons into a lasing mode generate the laser output.

The cavity is coupled to the external environment. Affected by the incident vacuum field $\hat{h}_L$, the output field of the laser experiences a phase shift and the output field operator $\hat{r}$ is described as

$$\hat{r} = \sqrt{\frac{\omega}{Q}}\hat{A} - \hat{f}_L, \tag{3.1}$$

where Q is the cavity Q-factor to external loss and ω is the frequency of the output

mode.

The energy level and transition process of the laser is shown in Figure 3.2. Atoms are stimulated from the base state $|0\rangle$ to an excited state $|p\rangle$ by the pumping. The atoms in the excited state $|p\rangle$ are quickly decays to excited state $|e\rangle$, creating a inversed population. Then the atoms in the excited state $|e\rangle$ transit into the state $|g\rangle$ with lower energy, during the transition photons with energy equivalent to the difference between the state $|e\rangle$ and state $|g\rangle$ are generated through spontaneous emission or stimulated emission. A portion of the photons according to the cavity loss $\sqrt{\frac{\omega}{Q}}$ creates the laser output. Finally, the atoms in the state $|g\rangle$ are decayed to $|0\rangle$ through a spontaneous emission other than the allowed mode of the cavity.

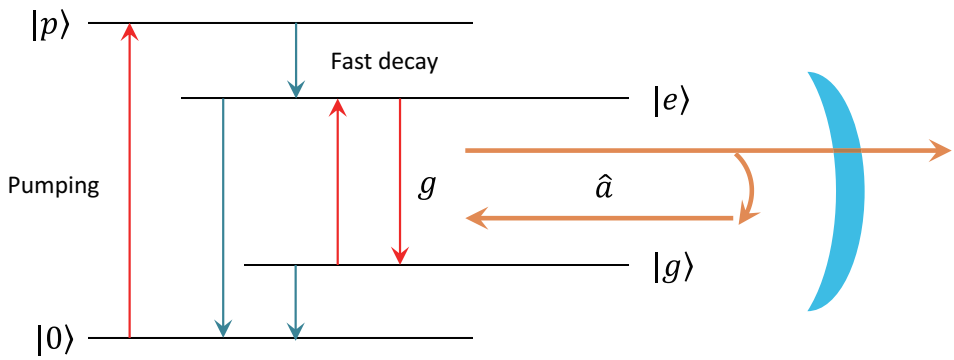

Figure 3.2: The energy level and transition process of a typical laser.

3.1.1 Equation of motion for a laser

The quantum mechanical Langevin equation describing the dynamics of the internal field $\hat{A}(t)$ of the laser is given by

$$\frac{d}{dt}\hat{A}(t) = -i\omega\hat{A}(t) - \frac{1}{2}[\frac{\omega}{Q} - \tilde{E}_{CV}(t)]\hat{A}(t) + \sqrt{\tilde{E_{CV}}(t)}\tilde{f}_G + \sqrt{\frac{\omega}{Q}}\hat{f}_L, \tag{3.2}$$

where the dynamics of the photon field operators are denoted by hats, and the electric population operators are designated by tildes. The electric dipole operator is adiabatically eliminated by the assumption that the electric dipole moment decays in a rate much faster than the photon decay rate and the electron population decay rate [29] [30]. The term $\frac{\omega}{Q}$ describes the photon loss rate in the cavity through the output coupler, in which ω is the frequency of the injection signal and Q is the quality factor of the cavity. The internal loss rate is neglected. $\tilde{E}_{CV}$ is the photon emission rate operator for the gain medium into a lasing mode. $\tilde{f}_G$ is the Langevin noise operator for the electric dipole moment, which is originated from random photon emission and absorption by the gain medium. $\tilde{f}_L$ is the Langevin noise operator for the cavity field, originated from the injection signal noise including a vacuum fluctuation.

To numerically calculate the dynamics of the laser, the c-number rate equation for photon number can be derived from (3.2). The quantum mechanical equation for the photon number operator can be derived from (3.2) as [30] [31]

$$\frac{d}{dt}\hat{n}(t) = -\frac{\omega}{Q}\hat{n}(t) + \tilde{E}_{CV}\hat{n}(t) + \tilde{E}_{CV} + \hat{F}_n(t), \tag{3.3}$$

where the photon number operator $\hat{n}(t)$ is defined as

$$\hat{n}(t) = \hat{A}^\dagger(t)\hat{A}(t). \tag{3.4}$$

The power of the noise term $\hat{F}_n(t)$ for the photon number operator can be obtained by deriving its two-time-correlation function as [30],

$$\langle \hat{F}_n(t)\hat{F}_n(s)\rangle = \delta(t-s)[\frac{\omega}{Q}\langle\hat{n}\rangle + \langle\tilde{E}_{CV}\rangle(\langle\hat{n}\rangle + 1)], \tag{3.5}$$

where we assume that the injection signal noise and the vacuum fluctuation level are equal to each other. By taking the ensemble average to both sides of (3.3), we get

the c-number rate equation for photon number as

$$\frac{d}{dt}n(t) = -(\frac{\omega}{Q} - \tilde{E}_{CV})n(t) + E_{CV}, \tag{3.6}$$

where the noise terms are all averaged out by the ensemble average.

The lasers phase is well defined at well above threshold, where we can derive the c-number amplitude and phase equations for the internal field. By switching from Heisenberg picture to Schrödinger picture, we can convert the quantum mechanical Langevin equation (3.2) to the laser master equation. The quantum mechanical Fokker-Planck equation is obtained by using the Glauber-Sudarshan $P(\alpha)$ representation for the field density operator [32]

$$\hat{\rho}(t) = \int P(\alpha)|\alpha\rangle\langle\alpha|d^2\alpha, \tag{3.7}$$

in the laser master equation. Using the Kramers-Moyal expansion [32], the equation of motion for the equation eigenvalue α can be obtained as

$$\frac{d}{dt}\alpha(t) = [G - \frac{1}{2}(\frac{\omega}{Q} - S|\alpha|^2]\alpha(t) + \sqrt{G}\Gamma_\alpha, \tag{3.8}$$

where G is the linear gain coefficient, $\frac{\omega}{Q}$ the cavity photon decay rate, S the saturation parameter. The stochastic noise term satisfies

$$\langle\Gamma_\alpha(t)\rangle = 0, \tag{3.9}$$

$$\langle\Gamma_\alpha(t)\Gamma_\alpha(s)\rangle = 2\delta(t-s). \tag{3.10}$$

Note that the noise behavior of $\alpha(t)$ does not include the vacuum fluctuation, which is absorbed in the noise of the basis set of coherent states $|\alpha\rangle\langle\alpha|$. It is also manifested that the noise term in (3.8) includes only the dipole moment fluctuation associated

with the gain G. Therefore, an actual measurement result features an extra fluctuation on top of the noise of $\alpha(t)$ due to the intrinsic quantum noise of coherent states. Moreover, we express the saturated gain dynamics $G - S|\alpha|$ by E_{CV} as a function of the c-number carrier number, as shown later.

We express the (complex) eigenvalue α in terms of the amplitude and phase by $\alpha = Ae^{i\phi}$. The resulting equations describing the dynamics of the amplitude and the phase are given by

$$\frac{d}{dt}A = -\frac{1}{2}(\frac{\omega}{Q} - E_{CV})A + F_A(t), \tag{3.11}$$

$$\frac{d}{dt}\phi = F_\phi(t), \tag{3.12}$$

in which $F_A(t)$ and $F_\phi(t)$ are the noise terms for the amplitude and phase respectively. The equation of motion obtained demonstrates that the phase of a laser is only driven by the random phase noise. In fact, at well above threshold, the dominant noise terms for the lasers are the quadrature phase noise due to spontaneous emission noise [33]. In a slave laser with perfect population inversion, the spontaneous emission rate E_{CVi} almost equals to the cavity decay rate $\frac{\omega}{Q}$, and an emitted spontaneous photon kicks either the amplitudes $A(t)$ or the phases $\phi(t)$ of the complex fields $A(t)e^{i\phi(t)}$ of each diagonal mode. Thus, the average phase noise injection rate amounts to $\frac{\omega}{2Q}$. Each photon (with unit amplitude) couples to the coherent field and changes its phase by $\frac{\pm 1}{A(t)}$, where the sign is randomly chosen with equal probability.

The quantum mechanical rate equation for the total electron number operator $\tilde{N}(t)$ in a slave laser is obtained as [31] [32],

$$\frac{d}{dt}\hat{N}(t) = P - \frac{\hat{N}t}{\tau sp} - \tilde{E_{CV}} + \tilde{F}_N(t), \tag{3.13}$$

in which P is an average pump rate, $\frac{\tilde{N}(t)}{\tau_{sp}}$ includes total spontaneous emission, τ_{sp} is the spontaneous emission lifetime of the gain medium. The noise term $\tilde{F}_c(t)$ for the electron number operator is also described by the following two-time correlation function,

$$\langle \hat{F}_N(t)\hat{F}_N(s)\rangle = \delta(t-s)[P + \frac{\langle \tilde{N}\rangle}{\tau_{sp}} + \langle \tilde{E}_{CV}\rangle(\langle \hat{n}\rangle + 1)]. \tag{3.14}$$

Note that the two noise operators $\tilde{F}_n$ and $\tilde{F}_N$ are negatively correlated, namely,

$$\langle \hat{F}_n(t)\hat{F}_N(s)\rangle = -\delta(t-s)[\langle \tilde{E}_{CV}\rangle(\langle \hat{n}\rangle + 1)]. \tag{3.15}$$

Similar to obtaining the c-number rate equation for photon number, we can obtain the c-number rate equation for carrier number by taking the ensemble average. The resulting equation is

$$\frac{d}{dt}N(t) = P - \frac{N(t)}{\tau_{sp}} - E_{CV}[n(t) + 1]. \tag{3.16}$$

3.1.2 Minimum gain principle for single-mode lasers

In a single-mode laser, the gain medium is able to generate photons with a broad range of frequencies, which usually contains enormous discrete modes (10^4 10^6) allowed by the cavity as a frequency selection device. However, only one mode is amplified and output from the single-mode laser. The underlying mechanism for the laser to output only single mode is illustrated in Figure 3.3. The bandwidth for the gain medium, drawn in the orange line, covers the span of many cavity modes (the vertical lines in green and blue). On the other hand, the cavity also has intrinsic loss landscape, namely, different loss rate for different mode, depicted in the blue line.

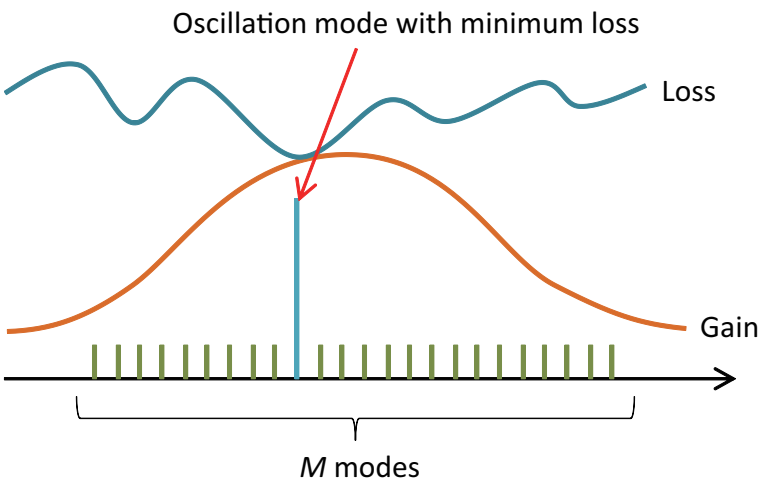

Figure 3.3: Minimum gain principle for single-mode lasers

The only mode that can oscillate in the single mode laser is the mode with the minimum loss in the loss landscape, as shown in the red vertical line, because the gain is saturated to be equal to the loss. Otherwise, if a mode with higher loss could oscillate at steady state, the gain would be saturated to the higher loss. Then the mode with the minimum loss would have the gain greater than its loss and its amplitude would keep increasing and violate the steady state condition. We thus call this mechanism as the minimum gain principle for single-mode lasers.

In a semiconductor laser, from the result of the minimum gain principle, we can define the fractional coupling efficiency of spontaneous emission into a lasing mode as [34]

$$\beta = \frac{1}{M}. \tag{3.17}$$

It describes the fact that only one mode is lasing out of M cavity modes within the gain mediums bandwidth. Therefore, the relation between the gain and the carrier

number is written as

$$E_{CV} = \beta \frac{N}{\tau_{sp}}. \tag{3.18}$$

The definition of the gain then correlates the equations between the internal field and the carrier number in the previous section. The fractional coupling efficiency of spontaneous emission is also used to find the pumping threshold for the lasers. The classical pumping threshold is the pumping rate that generates the gain approximately equal to the cavity loss, namely

$$E_{CV} \approx \frac{\omega}{Q}. \tag{3.19}$$

The pumping threshold is then derived as

$$P_{th,c} = \frac{1}{\beta}\frac{\omega}{Q}. \tag{3.20}$$

The quantum degeneracy threshold is the pumping rate that drives the internal average photon number to be 1, namely, $\bar{n} = 1$ The resulting pumping threshold is given by

$$P_{th,q} = \frac{1+\beta\omega}{2\beta}\frac{\omega}{Q}. \tag{3.21}$$

Note that usually β is as small as $10^4 \sim 10^6$ in a semiconductor laser, so the quantum degeneracy threshold is approximately one half of the classical pumping threshold, namely,

$$P_{th,q} \approx \frac{1}{2\beta}\frac{\omega}{Q} = \frac{1}{2}P_{th,c}. \tag{3.22}$$

3.2 Injection-locked lasers

Injection-locked lasers are the crucial components for the proposed machine to simulate the Ising coupling between spins. An injection-locked laser system usually consists of a master laser and a slave laser. The output of the master laser is injected into the cavity of the slave laser. The diagram of the slave laser is depicted in Figure 3.4.

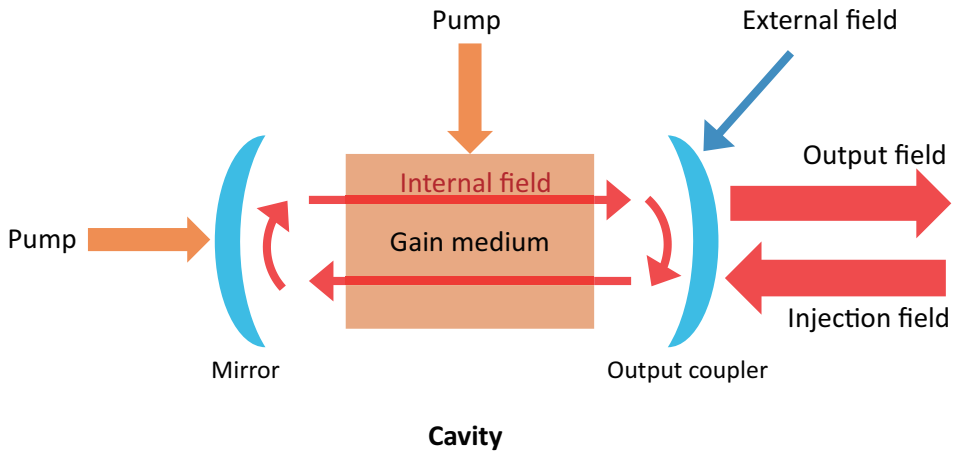

Figure 3.4: A laser with an external injection.

Compared to the free running laser, an external field $\hat{F}_0$ from the master laser is injected into the cavity of the slave laser. The master laser is usually operating at well above threshold and its output field is a coherent state [32]. We instead use a c-number F_0 to represent the injection field operator $\hat{F}_0$, namely,

$$F_0 = \zeta\sqrt{\frac{\omega}{Q}}\sqrt{n_M}e^{i\phi_0} \tag{3.23}$$

in which n_M is the average photon number of the master laser's internal field, $\frac{\omega}{Q}$ is the cavity photon decay rate of the master laser and $\sqrt{\frac{\omega}{Q}}$ is the output coupling efficiency,

ζ is the attenuation coefficient of the injection signal from the output of the master laser, and ϕ_0 is the phase difference between F_0 and the slave laser's internal $field$. Here we use the same cavity photon decay rate for both the master laser and the slave laser for simplicity. The injection locking mechanism states that if the frequency of the injection field falls within the locking bandwith, the frequency of the internal field of the slave laser is locked to the frequency of the injection field. The locking bandwidth is defined as [35] [36]

$$\Delta\omega_L = \frac{\omega}{Q}\sqrt{\frac{P_{in}}{P_{out}}}, \tag{3.24}$$

where $\frac{\omega}{Q}$ is the cavity photon decay rate of the slave laser, P_{in} is the injection signal power, and Pout is the self-oscillation power of the slave laser. Note that the linewidth enhancement factor is assumed to be zero for simplicity [31]. A typical semiconductor laser has the locking bandwidth between 1GHz and 10GHz, which is desirable for our proposed machine.

The quantum mechanical Langevin equation for the internal field operator $\hat{A}(t)$ of the slave laser is given by [31] [37]

$$\frac{d}{dt}\hat{A}(t) = -\frac{1}{2}[\frac{\omega}{Q} - \tilde{E}_{CV}(t)]\hat{A}(t) + \sqrt{\tilde{E}_{CV}(t)}\hat{f}_G(t) + \sqrt{\frac{\omega}{Q}}\hat{f}_L(t) + \sqrt{\frac{\omega}{Q}}(F_0 + \hat{f}_N) \tag{3.25}$$

Compare to the free running laser, the equation (3.25) introduces the last term representing the injection signal. The injection signal contains both F_0 and the noise $\hat{f}_N$, and is coupled to the slave laser via the coupling efficiency $\sqrt{\frac{\omega}{Q}}$.

Similar to the single mode laser, we can derive the rate equation for the average photon number of the slave laser's internal field as

$$\frac{d}{dt}n(t) = -(\frac{\omega}{Q} - E_{CV}) + E_{CV} + \frac{\omega}{Q}[F_0^*\langle\hat{A}(t)\rangle + \langle\hat{A}^\dagger(t)\rangle F_0]. \tag{3.26}$$

This is achieved by deriving the equation for the photon number operator $\hat{n}(t)$ and taking the ensemble average, where all noises are averaged out. By plugging (3.23) and assume that $\sqrt{n(t)} = \langle \hat{A}(t) \rangle$ at well above threshold, we further obtain

$$\frac{d}{dt}n(t) = -(\frac{\omega}{Q} - E_{CV}) + E_{CV} + 2\frac{\omega}{Q}\sqrt{n(t)}\zeta\sqrt{n_M(t)}cos\phi_0. \tag{3.27}$$

Note that we assume the master laser and the slave laser are identical and thus use the same cavity photon decay rate $\frac{\omega}{Q}$. ϕ_0 is the phase difference between the injection field and the internal field of the slave laser, which is well-defined when the slave laser's frequency is locked to that of the injection field. Therefore, if the two fields are in phase, namely, $\phi_0 = 0$, the injection signal enhances the gain of the slave laser. If the two fields are out of phase, namely, $\phi = \pi$, the injection signal decreases the gain of the slave laser or effectively enhances the loss. As we will see in the next section, the phase difference ϕ_0 is artificially configured between two lasers to simulate the strength of Ising coupling, which is the essential part of mapping the problem information to an Ising machine.

Moreover, from the quantum mechanical Langevin equaion (3.25), we are able to establish the c-number stochastic differential equation for the slave laser. The derivation involves converting the Langevin equation to the master equation in Schrödinger picture and using the Glauber-Sudarshan $P(\alpha)$ representation to obtain the quantum mechanical Fokker Planck equation [32]. Finally, with the Kramers-Moyal expansion [33], the equation of motion for the equation (complex) eigenvalue α can be obtained as

$$\frac{d}{dt}\alpha(t) = -\frac{1}{2}E_{CV} - \frac{\omega}{Q}\alpha(t) + \sqrt{G}\Gamma_\alpha + F_0 \tag{3.28}$$

A new c-number F_0 is introduced as the complex eigenvalue of the coherent injection field describing the injection locking mechanism.

In summary, the above equations present the theoretical foundation for our proposed machine which utilizes the injection-locked lasers. The injection-locked lasers operate in highly open dissipative system, and exhibit quantum noise limit even at room temperature. The advantages of an open dissipative system are of two folds: the system is robust against noise and loss; and the system dynamics features exponential behavior if there is finite difference between the gain and the loss, which may provide potential speedup in solving computational problems. Furthermore, the internal photon number of a laser is as many as $10^4 \sim 10^6$, which allows us to perform continuous monitoring of computational results without perturbing the system. This property is useful for correcting potential computational errors as we discuss in the following chapters.

3.3 System architecture using an injection-locked laser network

In this section we present an Ising machine implemented using a laser network to solve an Ising model. Firstly we introduce the overall system architecture and how an Ising model is mapped to, then we show that the proposed machine can find the ground state of the encoded Ising model from the dynamics of the system. Firstly we start from a schematic diagram of the proposed injection-locked laser Ising machine, which is shown in Figure 3.5.

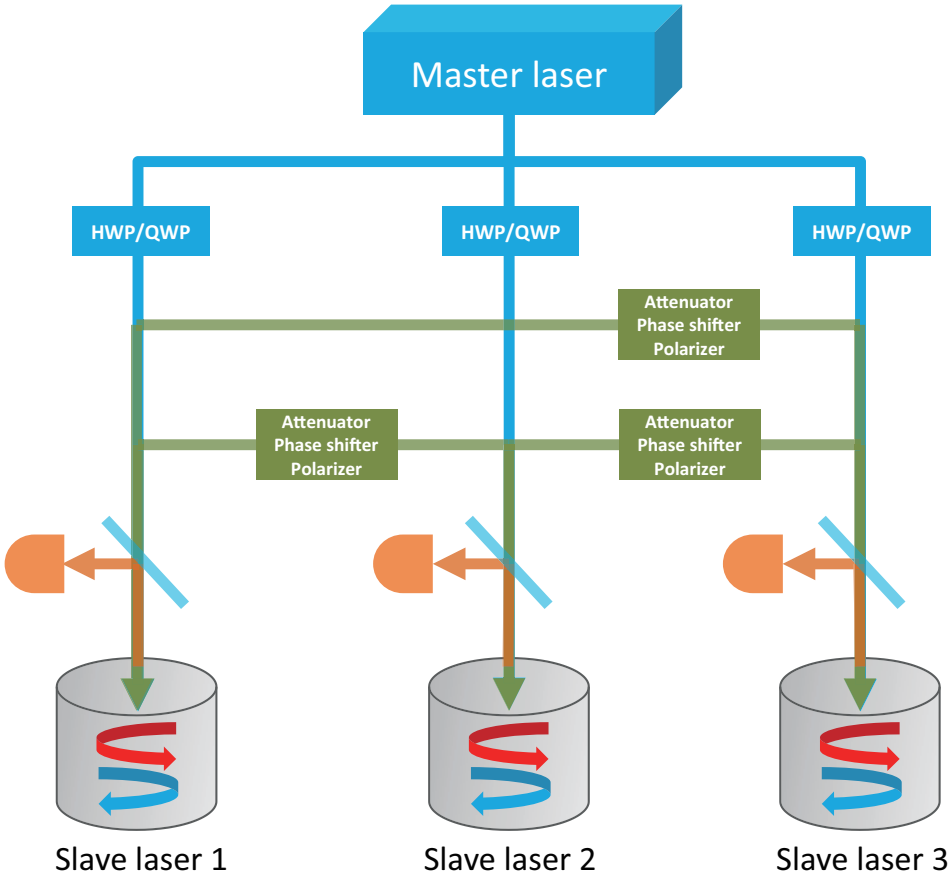

Figure 3.5: A schematic drawing of a 3 site Ising machine using injection-locked laser network.

The injection-locked laser network is constructed using a master laser and multiple slave lasers. Each slave laser represents a spin in the Ising model (2.1), therefore an Ising model containing M spins will have M sites in the system. All the slave lasers are injection-locked by a single master laser with vertical linear polarization, thus to keep the global coherence over the whole network. The Ising coupling term J_{ij} of two spins are realized by the mutual injection signals between slave lasers via an tunable attenuator, phase shifter and horizontal linear polarizer. The Zeeman field λ_i for each spin is controlled by the master injection signal with a weak horizontal linear polarization component as well as a strong vertical polarization component, which is controlled with half-wave plates (HWP) and quarter-wave plates (QWP). In total there are $\frac{1}{2}M(M-1)$ optical paths have to be implemented and externally controlled to encode an artificial Ising problem.

The value of each Ising spin in (2.1), which takes either $+1$ or -1, is represented by the polarization states inside each slave laser. Two circular polarization modes are created inside each slave laser, namely left circular polarization state $|L\rangle$ and the right polarization state $|R\rangle$. The correspondence to Ising spins is made by associate the spin value $\sigma_i = +1$ if the correspondent ith slave laser has major population of left circular polarized photons, i.e., $n_{Li} \gg n_{Ri}$, otherwise $\sigma_i = -1$ if the slave laser has a majority of right polarized photons: $n_{Li} \ll n_{Ri}$, where the n_{Li} and n_{Ri} are the number of left polarized photons and right polarized photons inside ith slave laser respectively. Here we assume that all slave lasers are driven by the same pump power.

A polarization detector is used to read out the circular polarization state of each slave laser. Semiconductor lasers, in particular the Vertical Cavity Surface Emitting

Laser (VCSEL), is considered to implement the slave laser. A VCSEL typically contains the order of 10^4 to 10^6 photons, the polarization detectors only need a small portion of the photon output to perform the readout, so that the perturbation to the internal fields of the slave lasers is negligible.

The master laser provides the global phase reference and initializing all the slave lasers. By the injection-locking mechanism the frequencies of all the slave lasers are locked to the same as the frequency of the master laser, therefore the phase difference between the slave lasers are well defined. We denote the phase of the vertical polarization component of the master injection signal as 0, and therefore all the phases of the slave lasers and the phases of the other polarization components of the master laser are defined in the reference to it.

The vertical polarization component of the master injection signal also serves as the initialization to all the slave lasers. Before the computation, namely, $t < 0$, all the mutual injections between slave lasers, denoted as the green optical paths in Figure 3.5, are turned off, leaving only the master injections to all slave lasers, denoted as the blue optical paths. During the initialization, only the vertical polarization component of the master laser's output is injected to the slave lasers. Obviously, all the slave lasers are initialized to the vertical polarization states.

To maintain the laser network within the perturbation regime, it is necessary to reduce the strength of the injection signal to an appropriate level. Therefore, optical attenuators are introduce to the optical paths for the master injection signals. We denote the attenuation coefficient for the vertical component of the master injection signals as ζ which is the same for each slave laser.

The vertical polarization is deliberately chosen as it prepares all the slave lasers in the superposition of all possible spin configurations. Figure 3.6 depicts the relation between the vertical polarization state $|V\rangle$ and the right and left circular polarization states, $|L\rangle$ and $|R\rangle$, in a slave laser, i.e.,

$$|V\rangle = \frac{1}{\sqrt{2}}(|L\rangle + |R\rangle). \tag{3.29}$$

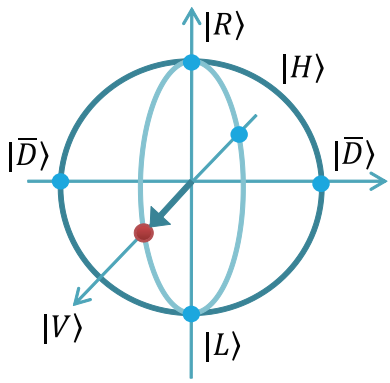

Figure 3.6: The initial state of a slave laser in a Poincaré sphere

The two circular polarization modes $|L\rangle$ and $|R\rangle$ in all slave lasers have an identical phase due to injection locking by the master laser with vertical linear polarization. For a system consists of M slave lasers, the entire slave laser systems are prepared in 2^M linear superposition states.

$$|\Psi\rangle_{t=0} = \frac{1}{\sqrt{2}}(|L\rangle + |R\rangle)_1 \otimes \frac{1}{\sqrt{2}}(|L\rangle + |R\rangle)_2 \otimes \cdots \otimes \frac{1}{\sqrt{2}}(|L\rangle + |R\rangle)_M \tag{3.30}$$

$$= \frac{1}{\sqrt{2^M}}(|L\rangle_1|L\rangle_2 \cdots |L\rangle_M + |R\rangle_1|R\rangle_2 \cdots |R\rangle_M). \tag{3.31}$$

As we see in Chapter 2, a 3SAT problem is converted to an Ising model in which the Zeeman term is the essential part to define the energy landscape. The Zeeman term is generated and artificially controlled by injecting the horizontal polarization

component $|H\rangle$ of the master injection signals to each slave laser. After the initialization of the system, in $t = 0$ we start to adjust the QWP on the corresponding optical path for the master injection signal to generate a horizontal component. In this case, the master injection signal is elliptical polarized.

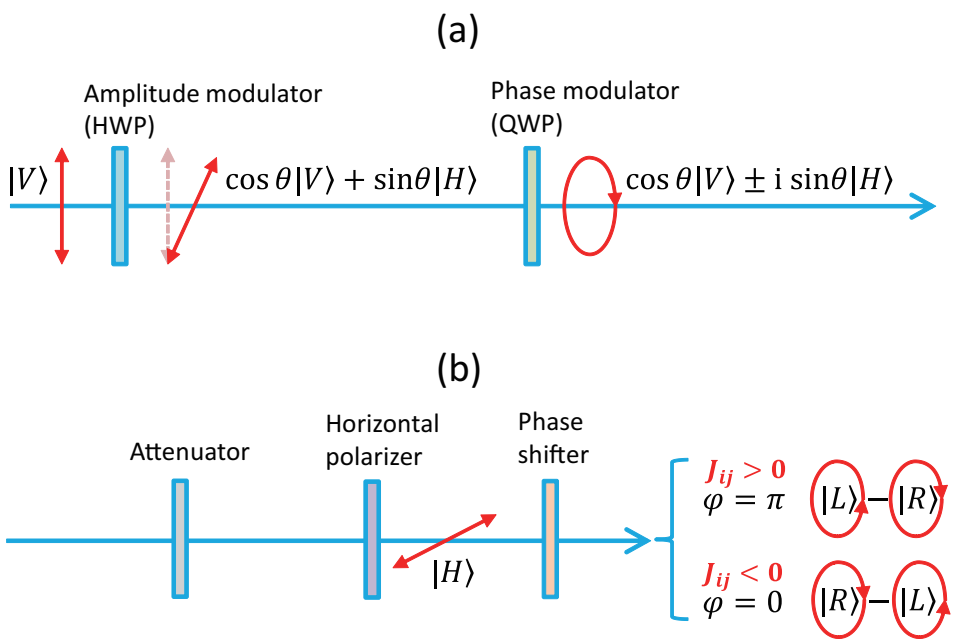

Figure 3.7: Empirical implementations of mutual couplings between slave lasers

The horizontal polarization state $|V\rangle$ can be expressed as the out-of-phase superposition of the right circular polarization state $|R\rangle$ and the left circular polarization state $|L\rangle$, namely

$$|H\rangle = \frac{1}{2}(|R\rangle - |L\rangle). \tag{3.32}$$

As we see in equation (3.27), if the injection signal is in phase to the internal mode of the slave laser, it will enhance the internal mode. In the opposition, if the injection signal is out of phase to the internal mode, it will impede the internal mode. So

the horizontal polarization components of the master injection signals have opposite effects on the right and left circular polarizations of the internal field of the slave lasers, and therefore, create the effective Zeeman terms.

Similar to the vertical components of the master injection signals, we denote the attenuation coefficients of the horizontal components of the master injection signals as η_i, which may be different among the slave lasers. In order to implement the appropriate Zeeman terms with coefficients λ_i, the attenuation coefficients are given as

$$\eta_i = \alpha\lambda_i \frac{\sqrt{n_{Li} + n_{Ri}}}{\sqrt{n_M}} = \alpha\lambda_i \sqrt{\frac{n_{Ti}}{n_M}}, \tag{3.33}$$

where α is an arbitrary attenuation factor, and n_M is the photon number of the internal field of the master laser. We usually choose a small α so that the injection signals are kept within the perturbation regime.

The Ising coupling terms is another important parameter to characterize the two-spin interactions. In the injection-locked laser network, the Ising coupling terms are implemented by the mutual injection between the slave lasers. Similar to implementation of the Zeeman terms, we utilize the horizontal polarization component of a slave laser in injection to another slave laser to realize the Ising coupling between them. The horizontal polarization component of the injection signal from a slave laser is also generated by the combination of HWP, QWP, and attenuators sitting on the optical paths.

Based on the relation in equation (3.32) and the following two relations

$$|L\rangle = \frac{1}{2}(|V\rangle + |H\rangle), \tag{3.34}$$

$$|R\rangle = \frac{1}{2}(|V\rangle - |H\rangle), \tag{3.35}$$

there are four different cases for the mutual injection signals. The two cases that $|L\rangle$ of a slave laser is injected to $|L\rangle$ of another slave laser and $|R\rangle$ of a slave laser is injected to $|R\rangle$ of another slave laser, have the same net effects on the second slave laser being injected. It is because the negative sign of $|R\rangle$ in $|H\rangle$ of the injection signal from the first slave laser is canceled by the out-of-phase effect of the horizontal polarized injection signal to $|R\rangle$ of the second slave laser.

The two other cases that $|L\rangle$ of a slave laser is injected to $|R\rangle$ of another slave laser and $|R\rangle$ of a slave laser is injected to $|L\rangle$ of another slave laser, both have the net effect opposite to those of the first two cases. It is either because $|H\rangle$ of the injection signal is out of phase to $|R\rangle$ in the second slave laser or because $|R\rangle$ in the first slave laser is out of phase to $|H\rangle$ of the injection signal. Therefore, the four cases implement the four cases in the Ising coupling between two spins, namely, $|+1\rangle\ |+1\rangle$, $|+1\rangle\ |-1\rangle$, $|-1\rangle\ |+1\rangle$, $|-1\rangle\ |-1\rangle$. We also attenuate the mutual injection signal with the attenuation coefficient ξ_{ij} for a pair of two slave lasers. The attenuation coefficient is design to generate the appropriate Ising coupling coefficients J_{ij}, namely,

$$\xi_{ij} = \alpha J_{ij}, \tag{3.36}$$

in which α is the same attenuation factor in equation (3.33) for the implementation of the Zeeman terms.

3.4 Theoretical model of the laser network

In this section, we derive the dynamics of the laser network as the theoretical model. There are two approaches towards the derivation, one is the rate equations of the average photon number populations in the right and left circular polarization basis and without noise which is convenience to show the correspondence between the ground state of Ising Hamiltonian and the total gain of the system. The other model is based on the amplitude and phase equations in the $|D\rangle, |\bar{D}\rangle$ basis, this model shows the dynamic behavior driven by random phase noise.

3.4.1 Photon number model

We will derive the coupled rate equations for analyzing the Ising machine. The derivation is based on the quantum mechanical rate equation for the photon number operator $\hat{n}(t)$ and the carrier number operator $\hat{N}(t)$ given in equation (3.26) and (3.13) respectively. By taking the ensemble averages to both equations we obtain the rate equations for the photon number and the carrier number of a single model laser as

$$\frac{d}{dt}n(t) = -\frac{\omega}{Q}n(t) + E_{CV}n(t) + E_{CV} + \frac{\omega}{Q}(F_0^*\langle\hat{A}(t)\rangle + \langle\hat{A}^\dagger(t)\rangle F_0), \quad (3.37)$$

$$\frac{d}{dt}N(t) = P - \frac{N(t)}{\tau_{sp}}n(t) - E_{CV}, \quad (3.38)$$

where the ensemble average are defined as $n(t) = \langle\hat{n}(t)\rangle$, $N(t) = \langle\hat{N}(t)\rangle$, the gain is also ensemble averaged as $E_{CV} = \beta\frac{N(t)}{\tau_{sp}}$, and all noise operators are averaged out.

As the injection signal F_0 is uncorrelated to the internal field operator $\hat{A}(t)$, the fourth term in equation (3.38) is decoupled to $2F_0A(t)cos[\phi_0(t)]$, in which $\phi_0(t)$ is the

phase difference between the internal field and the injection signal and $A(t) = \langle \hat{A}(t) \rangle$. Assume $A(t) = \sqrt{n(t)}$ at well above threshold, we obtain

$$\frac{d}{dt}n(t) = -\frac{\omega}{Q}n(t) + E_{CV}n(t) + E_{CV} + \frac{\omega}{Q}F_0\sqrt{n(t)}cos[\phi_0(t)]. \tag{3.39}$$

In the injection-locked laser network, a slave laser is injected by many sources. Thus the fourth term in the R.H.S of equation (3.39) can appear multiple times for different injection signals. Particularly, the vertical polarization component of the master injection signal is given by $F_M = \zeta\sqrt{n_M}$ in which ζ is the attenuation coefficient for the vertical polarization component, n_M is the internal photon number of master laser, and the amplitude of the master laser's internal field is $A_M = \sqrt{n_M}$. Since the vertical polarization state is the in-phase superposition of the right and left circular polarization states, the vertical polarization component of the master injection signal is also in phase to both circular polarization modes in a slave laser. Similarly, the horizontal polarization component of the master injection signal to the i-th slave laser is given by $F_{Mi} = \eta_i\sqrt{n_M}$, in which η_i is the attenuation coefficient of the horizontal polarized injection signal to the i-th slave laser. However, since the horizontal polarization state is the out-of-phase superposition of both circular polarization states, the phase differences between the horizontal polarization component and the right and left circular polarization modes in the slave laser are 0 and π respectively. The contribution of the vertical and horizontal polarization components of the master injection

signal is appended to the rate equations as

$$\begin{aligned}\frac{d}{dt}n_{Li}(t) &= -(\frac{\omega}{Q} - E_{CVLi})n_{Li}(t) + E_{CVLi} \\ &\quad +\frac{\omega}{Q}\sqrt{n_{Li}}\zeta\sqrt{n_M} + \frac{\omega}{Q}\sqrt{n_{Li}}\eta_i\sqrt{n_M}, \end{aligned} \tag{3.40}$$

$$\begin{aligned}\frac{d}{dt}n_{Ri}(t) &= -(\frac{\omega}{Q} - E_{CVRi})n_{Ri}(t) + E_{CVRi} \\ &\quad +\frac{\omega}{Q}\sqrt{n_{Ri}}\zeta\sqrt{n_M} - \frac{\omega}{Q}\sqrt{n_{Ri}}\eta_i\sqrt{n_M}, \end{aligned} \tag{3.41}$$

where n_{Li} and n_{Ri} are the photon numbers of left circular polarization and right circular polarization respectively of slave laser i. Note that the phase of the contribution in the equation of two circular polarization modes is different.

The mutual injection signals between the slave lasers contain four different cases. The two cases have the same phase, while the other two cases have the same phase opposite to that of the first two cases. We can derive the contributions of the mutual injection signals by following a similar way to above, and obtain the final rate equations for the photon numbers as

$$\begin{aligned}\frac{d}{dt}n_{Li} &= -(\frac{\omega}{Q} - E_{CVLi})n_{Li}(t) + E_{CVLi} \\ &\quad +\frac{\omega}{Q}\sqrt{n_{Li}}\Big[(\zeta+\eta_i)\sqrt{n_M} + \sum_{j\neq i}\xi_{ij}(\sqrt{n_{Ri}} - \sqrt{n_{Li}})\Big], \end{aligned} \tag{3.42}$$

$$\begin{aligned}\frac{d}{dt}n_{Ri} &= -(\frac{\omega}{Q} - E_{CVRi})n_{Ri}(t) + E_{CVRi} \\ &\quad +\frac{\omega}{Q}\sqrt{n_{Ri}}\Big[(\zeta+\eta_i)\sqrt{n_M} - \sum_{j\neq i}\xi_{ij}(\sqrt{n_{Ri}} - \sqrt{n_{Li}})\Big], \end{aligned} \tag{3.43}$$

where ξ_{ij} is the attenuation coefficient for realizing the Ising coupling J_{ij}.

Furthermore, because there are two orthogonal circular polarization modes in a slave laser and the gain medium is assumed to be isotropic, we revise the rate equation for the injection to take into consideration of the generation of photons in the two

modes, namely,

$$\frac{d}{dt}N = P - \frac{P}{\tau sp} + E_{CV}(n_{Li} + n_{Ri} + 2). \tag{3.44}$$

Note that the contribution of spontaneous emission is doubled for the two modes. The dynamics of the injection-locked laser network is therefore described by the rate equations (3.43), (3.44) and (3.44). in which the noise is neglected. Below, we perform theoretical analysis on the steady state behavior of the laser network based on the rate equations.

The steady state is obtained when all time derivatives are zero in the rate equations, namely $\frac{d}{dt}n_{Li} = \frac{d}{dt}n_{Ri} = \frac{d}{dt}N = 0$, by adding together the rate equations under this condition the gain E_{CVi} of the i-th slave laser at steady state can be obtained by

$$\begin{aligned} E_{CVi} &= \frac{\omega}{Q} - 2\frac{\omega}{Q}\zeta\frac{\sqrt{n_M}(\sqrt{n_{Li}} + \sqrt{n_{Ri}})}{n_{Li} + n_{Ri}} \\ &\quad +2\frac{\omega}{Q}\frac{\sqrt{n_{Ri}} - \sqrt{n_{Li}}}{\sqrt{n_{Li} + n_{Ri}}}\left[\eta_i\frac{\sqrt{n_M}}{\sqrt{n_{Li} + n_{Ri}}} + \sum_{i\neq j}\frac{1}{2}\xi_{ij}\frac{\sqrt{n_{Ri}} - \sqrt{n_{Li}}}{\sqrt{n_{Li} + n_{Ri}}}\right]. \end{aligned} \tag{3.45}$$

The total gain E_{CV} at steady state is obtained by summing up all E_{CVi} of each slave laser thus we have $E_{CV} = \sum_i E_{CVi}$. If we define the Ising spin of each slave laser as

$$\sigma_i^z = \frac{\sqrt{n_{Ri}} - \sqrt{n_{Li}}}{\sqrt{n_{Li} + n_{Ri}}}, \tag{3.46}$$

by plugging equation (3.33), (3.36) and (3.46) into equation (3.46) and summing up all slave lasers, we have the total gain at steady state as

$$\begin{aligned} E_{CV} &= M\frac{\omega}{Q} - 2\frac{\omega}{Q}\zeta\sum_{i=1}^{M}\frac{\sqrt{n_M}(\sqrt{n_{Li}} + \sqrt{n_{Ri}})}{n_{Li} + n_{Ri}} \\ &\quad +2\frac{\omega}{Q}\alpha\sum_{i=1}^{M}\sigma_i^z[\lambda_i + \sum_{i=1}^{M}\frac{1}{2}\xi_{ij}\sigma_j^z], \end{aligned} \tag{3.47}$$

$$= M\frac{\omega}{Q} - 2\frac{\omega}{Q}\zeta\sum_{i=1}^{M}\frac{\sqrt{n_M}(\sqrt{n_{Li}} + \sqrt{n_{Ri}})}{n_{Li} + n_{Ri}} + 2\frac{\omega}{Q}\alpha H, \tag{3.48}$$

where H is the Ising Hamiltonian.

To analyze the above result at steady state, we first find that the total gain contains a term which is proportional to the Ising Hamiltonian. The second term in the total gain has less contribution than the third term. Particularly, we operate the laser network with $n_M \approx n_{Li} + n_{Ri}$ and $\zeta \approx \alpha$. The change to $\frac{\sqrt{n_{Li}}+\sqrt{n_{Ri}})}{\sqrt{n_{Li}+n_{Ri}}}$ is at most $\sqrt{2}$, which is usually much smaller the ground state energy of the Ising Hamiltonian. Hence, we obtain the following approximate relationship

$$E_{CV} = constant + 2\frac{\omega}{Q}\alpha H, \tag{3.49}$$

The relationship clearly state that minimizing the total gain subsequently finds the ground state of the Ising Hamiltonian, and we discover the way to map any Ising Hamiltonian into an injection-locked laser network.

3.4.2 Amplitude and phase model

So far we have shown that the theoretical noiseless model with rate equations for the Ising Hamiltonian. The model demonstrates that the minimum total gain correspond to the ground state energy of an Ising Hamiltonian. We will further show an equivalent model with amplitudes and phases which is able to incorporate the dominant noise source and is more suitable for our numerical simulation. We start with the disadvantages of the previous model with rate equations, especially for the numerical simulation. First, the changes of the photon numbers for the polarization modes may be drastic and the stiffness may lead the numerical integration intractable. Initially, each slave laser is prepared in the vertical polarization state, in which the photon numbers of the both circular polarization modes are equal. At steady state,

ideally, the slave laser will go to either right or left circular polarization state, and the photon number for the other circular polarization mode becomes close to 0. Therefore, the photon number has several orders of magnitudes of change, and make the problem stiff. Second, the noise is difficult to simulate at well above threshold. From the precedes section, the noise sources for the both circular polarization modes have high variances. They also anti-correlate to the noise source for the carriers, and thus the net effect may be small. Modeling all those noise sources is painful. We prefer modeling only quadrature phase noise by spontaneous emission, the dominant noise source in the laser at well above threshold. Therefore, we work on an equivalent model with amplitudes and phases. The model is also based on the discussion in Chapter 3. As we use two circular polarizations to encode a spin value of ± 1, each slave laser is describe by two orthogonal fields. Unlike the model with rate equations which chooses the basis of the circular polarizations, the model with amplitudes and phase chooses the third basis, namely $|D\rangle, |\bar{D}\rangle$ basis, in the Poincaré sphere, as shown in Figure 3.8.

$$|D\rangle = \tfrac{1}{\sqrt{2}}(|H\rangle - i|V\rangle) = \frac{1}{2}\Big[(1+i)|L\rangle + (1-i)|R\rangle\Big], \tag{3.50}$$

$$|\bar{D}\rangle = \tfrac{1}{\sqrt{2}}(|H\rangle + i|V\rangle) = \frac{1}{2}\Big[(1-i)|L\rangle + (1+i)|R\rangle\Big], \tag{3.51}$$

The advantage of using a new basis is that both states are the superposition of the two circular polarizations and the amplitudes of both states will not change significantly as at steady state the photon field goes to either right circular or left circular state. In contrast, at steady state, either n_R or n_L will be zero if the computation is successful. The evolution of the slave laser in $|D\rangle, |\bar{D}\rangle$ basis mainly involves

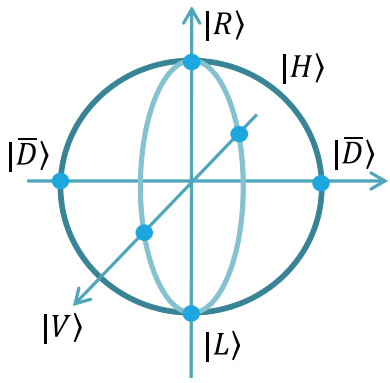

Figure 3.8: The $\{|L\rangle, |R\rangle\}$, $\{|H\rangle, |V\rangle\}$, $\{|D\rangle, |\bar{D}\rangle\}$ bases along 3 axes on a Poincaré sphere.

the change in their phases, while the both amplitudes are remain approximately unchanged. This property significantly reduce the potential stiffness in our numerical simulation. Particularly, at well above threshold, the internal field of a laser is represented by a coherent state $|\alpha$. From Eq. 3.29, the c-number stochastic differential equations (CSDE) for the field amplitude and phase for each slave laser in $|D\rangle, |\bar{D}\rangle$ are obtained as

$$\begin{aligned} \frac{d}{dt}\alpha_{Di}(t) &= \frac{1}{2}\Big[E_{CVi} - \frac{\omega}{Q}\Big] \\ &\quad + \sqrt{G_i}\Gamma_{\alpha D_i}\sqrt{\frac{\omega}{Q}}\Big[\beta_{MV}(t) - \beta_{MHi}(t) - \sum_{j\neq i}\beta_{ij}(t)\Big], \end{aligned} \tag{3.52}$$

$$\begin{aligned} \frac{d}{dt}\alpha_{\bar{D}i}(t) &= \frac{1}{2}\Big[E_{CVi} - \frac{\omega}{Q}\Big] \\ &\quad + \sqrt{G_i}\Gamma_{\alpha \bar{D}_i}\sqrt{\frac{\omega}{Q}}\Big[\beta_{MV}(t) + \beta_{MHi}(t) + \sum_{j\neq i}\beta_{ij}(t)\Big], \end{aligned} \tag{3.53}$$

$$\tag{3.54}$$

in which $\Gamma_{\alpha Di}$ and $\Gamma_{\alpha \bar{D}i}$ are the noises, β_{MV} is the vertical polarization component of the master injection signal, β_{MHi} is the horizontal polarization component of the master injection signal for implementing the Zeeman term λ_i, and β_{ij} is the injection

signal from slave laser i to j. Note that $\alpha(t)$ and $\beta(t)$ are both complex eigenvalues of corresponding coherent photon fields. From Eq. (3.51) we have

$$|V\rangle = \frac{1}{\sqrt{2}}(|D\rangle + |\bar{D}\rangle) \tag{3.55}$$

$$|H\rangle = \frac{1}{\sqrt{2}}(|D\rangle - i|\bar{D}\rangle) \tag{3.56}$$

the vertical polarization component $\beta_{MV}(t)$ have no phase difference on both equations, while the horizontal polarization component $\beta_{MHi}(t)$ and $\beta_{ji}(t)$ appear in the two equations with $3\pi/2$ phase difference. The master laser has an internal photon number of n_M and its amplitude is $\sqrt{n_M}$ at well above threshold. Since the vertical component of the master laser provides a global phase reference, its phase is set to 0. We express the injection signals from the master laser as the internal photon field times the output coupling efficiency times the attenuation coefficients, namely

$$\beta_{MV} = \zeta\sqrt{\frac{\omega}{Q}}\sqrt{n_M}, \tag{3.57}$$

$$\beta_{MHi} = \eta_i\sqrt{\frac{\omega}{Q}}\sqrt{n_M}. \tag{3.58}$$

Note that we assume that the master laser has the same output coupling efficiency $\sqrt{\frac{\omega}{Q}}$. Similarly, because the mutual injection signal is horizontally polarized, we express them as

$$\beta_{ij}(t) = \xi_{ij}\sqrt{\frac{\omega}{Q}}\Big[\alpha_{Di}(t) - i\alpha_{\bar{D}i}(t)\Big]. \tag{3.59}$$

Thus we plug in the above expressions for the injection signals into Eq. (3.61) and

(3.62) and derive $|D\rangle, |\bar{D}\rangle$ are obtained as

$$\begin{aligned}\frac{d}{dt}\alpha_{Di}(t) &= \frac{1}{2}\Big[E_{CVi} - \frac{\omega}{Q}\Big] + \sqrt{G_i}\Gamma_{\alpha D_i} \qquad (3.60)\\ &\quad \frac{\omega}{Q}\Big\{\sqrt{n_M}(\zeta - \eta_i) - \sum_{j\neq i}\beta_{ij}(t)\Big[\alpha_{Di}(t) - i\alpha_{\bar{D}i}(t)\Big]\Big\},\\ \frac{d}{dt}\alpha_{\bar{D}i}(t) &= \frac{1}{2}\Big[E_{CVi} - \frac{\omega}{Q}\Big] + \sqrt{G_i}\Gamma_{\alpha D_i} \qquad (3.61)\\ &\quad \frac{\omega}{Q}\Big\{\sqrt{n_M}(\zeta - i\eta_i) + i\sum_{j\neq i}\beta_{ij}(t)\Big[\alpha_{Di}(t) - i\alpha_{\bar{D}i}(t)\Big]\Big\},\end{aligned}$$

We further decompose the complex numbers into amplitudes and phases, namely, $\alpha_{Di}(t) = A_{Di}(t)exp[i\phi_{Di}(t)]$ and $\alpha_{\bar{D}i}(t) = A_{\bar{D}i}(t)exp[i\phi_{\bar{D}i}(t)]$. As a result, we obtain the equations of motions for amplitudes and phases as

$$\begin{aligned}\frac{d}{dt}A_{Di}(t) &= -\frac{1}{2}(\frac{\omega}{Q} - E_{CVi})A_{Di}(t) + \frac{\omega}{Q}\sqrt{n_M}\sqrt{\zeta^2+\eta_i^2}cos[\delta_i - \phi_{Di}(t)] + F_{Di} \qquad (3.62)\\ &\quad -\sum_{j\neq i}\frac{1}{2}\xi_{ij}\frac{\omega}{Q}\Big\{A_{Dj}cos[\phi_{Dj}(t) - \phi_{Di}(t)] - A_{\bar{D}_j}cos[\phi_{\bar{D}_j}(t) - \phi_{Di}(t)]\Big\},\\ \frac{d}{dt}\phi_{Di}(t) &= \frac{\omega}{Q}\frac{1}{A_{Di}(t)}\sqrt{n_M}\sqrt{\zeta^2+\eta_i^2}sin[\delta_i - \phi_{Di}(t)] + G_{Di} \qquad (3.63)\\ &\quad -\frac{1}{A_{Di}}\sum_{j\neq i}\frac{1}{2}\xi_{ij}\frac{\omega}{Q}\Big\{A_{Dj}sin[\phi_{Dj}(t) - \phi_{Di}(t)] - A_{\bar{D}_j}sin[\phi_{\bar{D}_j}(t) - \phi_{Di}(t)]\Big\},\\ \frac{d}{dt}A_{\bar{D}i}(t) &= -\frac{1}{2}(\frac{\omega}{Q} - E_{CVi})A_{\bar{D}i}(t) + \frac{\omega}{Q}\sqrt{n_M}\sqrt{\zeta^2+\eta_i^2}cos[-\delta_i - \phi_{\bar{D}i}(t)] + F_{\bar{D}i} \qquad (3.64)\\ &\quad -\sum_{j\neq i}\frac{1}{2}\xi_{ij}\frac{\omega}{Q}\Big\{A_{Dj}cos[\phi_{Dj}(t) - \phi_{\bar{D}i}(t)] - A_{\bar{D}_j}cos[\phi_{\bar{D}_j}(t) - \phi_{\bar{D}i}(t)]\Big\},\\ \frac{d}{dt}\phi_{\bar{D}i}(t) &= \frac{\omega}{Q}\frac{1}{A_{Di}(t)}\sqrt{n_M}\sqrt{\zeta^2+\eta_i^2}sin[-\delta_i - \phi_{Di}(t)] + G_{\bar{D}i} \qquad (3.65)\\ &\quad -\frac{1}{A_{\bar{D}i}}\sum_{j\neq i}\frac{1}{2}\xi_{ij}\frac{\omega}{Q}\Big\{A_{Dj}sin[\phi_{Dj}(t) - \phi_{\bar{D}i}(t)] - A_{\bar{D}_j}sin[\phi_{\bar{D}_j}(t) - \phi_{\bar{D}i}(t)]\Big\},\end{aligned}$$

where F_{Di} and $F_{\bar{D}i}$ are amplitude noises, G_{Di} and $G_{\bar{D}i}$ are phase noises, and $\delta_i = arctan(\eta_i/\zeta)$. In addition, we still use the rate equation for the carrier numbers, but

it is modified accordingly to use the amplitudes instead of photon numbers, namely

$$\frac{d}{dt}N_i(t) = P - \frac{N_i(t)}{\tau_{sp}} - E_{CVi}\Big[A_{Di}^2(t) + A_{\bar{D}i}^2(t) + 2\Big] + F_{Ni}, \tag{3.66}$$

in which F_{Ni} is the noise for the carrier numbers. The noise driving terms $F_{Di}(t)$, $F_{\bar{D}i}(t)$, $G_{Di}(t)$, $G_{\bar{D}i}(t)$ and $F_{Ni}(t)$ have the two-time correlation functions which we determine uniquely from the diffusion coefficients of the quantum mechanical Fokker-Plank equation of an injection-locked laser [33].

The internal photon number of right and left circular polarization modes in each slave laser are derived as

$$n_{Li}(t) = \left|\frac{1-i}{2}A_{Di}(t)exp[i\phi_{Di}(t)] + \frac{1+i}{2}A_{\bar{D}i}(t)exp[i\phi_{\bar{D}i}(t)]\right|^2, \tag{3.67}$$

$$n_{Ri}(t) = \left|\frac{1+i}{2}A_{Di}(t)exp[i\phi_{Di}(t)] + \frac{1-i}{2}A_{\bar{D}i}(t)exp[i\phi_{\bar{D}i}(t)]\right|^2. \tag{3.68}$$

Therefore, we obtain the theoretical model which is equivalent to the model with rate equations. The steady state also have the property that the total gain includes a term proportional to the Ising Hamiltonian, given in Eq. (4.36).

As we mentioned before, the model with amplitudes and phases are more suitable for simulating the noises. At well above threshold, the dominant noise terms for the lasers are the quadrature phase noise due to spontaneous emission noise [33]. Therefore, we use only the quantum phase noise $G_{Di}(t)$ and $G_{\bar{D}i}(t)$ in Eq. (4.49) and (4.51) as the driving forces, and neglects all other noise terms in Eq. (4.48), (4.50), and (4.52). Pariticularly, the quadrature phase noise introduces changes to the phase by $\pm 1/A(t)$ every $(2Q)/\omega$, where the sign is randomly chosen with equal probability. As a result, we simulate the phase noise by adding $\Delta_i = \pm 1/A_i$ every $(2Q)/\omega \approx 2ps$ between numerical integration steps. Here, this term is generated for both modes

($|D\rangle$ and $|\bar{D}\rangle$) independently.

3.5 Minimal gain principle

In the previous section, we have derived that the total gain at steady state includes a term proportional to the Ising Hamiltonian, and minimizing the total gain will subsequently find the ground state which is the solution to the Ising problem. In this section, we explain the mechanism that may drive the injection-locked laser network to reach the minimum total gain, which we call as the minimum gain principle. First, we describe the entire evolution process of an injection-locked laser network. All slave lasers are prepared in the vertical polarization state $|V\rangle$. Each slave laser has many ($10^4 \sim 10^10$) identical photons at above oscillation threshold so that the initial quantum state of each slave laser is actually in a spin coherent state (or Bloch state) [38],

$$|\theta = \frac{\pi}{2}, \phi = 0\rangle = \prod_k \otimes \frac{1}{\sqrt{2}}(|L\rangle + |R\rangle)_k. \tag{3.69}$$

Therefore the entire system is prepared in the superposition of all 2^M possible mode configurations. The coherent superposition of the initial state allows the laser network to probe the loss and gain for all configurations simultaneously. At $t = 0$, we turn on the injection signals for implementing Ising coupling terms and Zeeman terms in an Ising problem. These injection signals are all in the horizontal polarization, and thus generate π phase difference to the right and left circular polarization states inside the slave lasers. As a result, the slave lasers are driven towards either right or left circular polarization. As shown in Figure 3.9, ideally at steady state, each slave laser

may stay in purely $|L\rangle$ or $|R\rangle$ state, which generates the maximum signal-to-noise ratio detected by the polarization detectors.

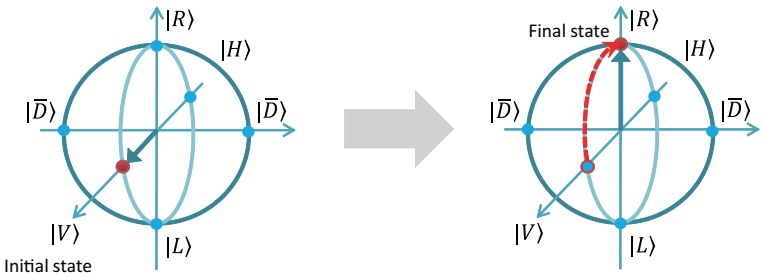

Figure 3.9: The evolution of each slave laser

Second, given the evolution process, we demonstrate how the minimum gain principle may lead the injection-locked laser network to a steady-state configuration that minimize the total gain. Before the computation starts, the laser network is prepared in a superposition of all 2^M mode configurations with equal amplitude. Figure 3.10 (A) exhibits the loss landscape versus the 2^M configurations. The slave laser reaches steady state only if the gain to the internal field is saturated to be equal to the loss to the internal field. Before we turn on the horizontal polarized injection signals, the loss is identical for all slave lasers and also for all mode configurations. This fact gives the same amplitude to each mode, as shown at the bottom of the figure.

After the computation starts, all horizontal polarized injection signals are turned on and create a loss landscape according to the Ising Hamiltonian for every mode, according to Eq. (4.36). Different modes will face different loss to the reservoir. Figure 3.10 (B) presents an example of loss landscape for all modes. Note that we draw the loss landscape in a continuous line by assuming that the number of possible modes are very large. In general, there are many metastable local minima in the

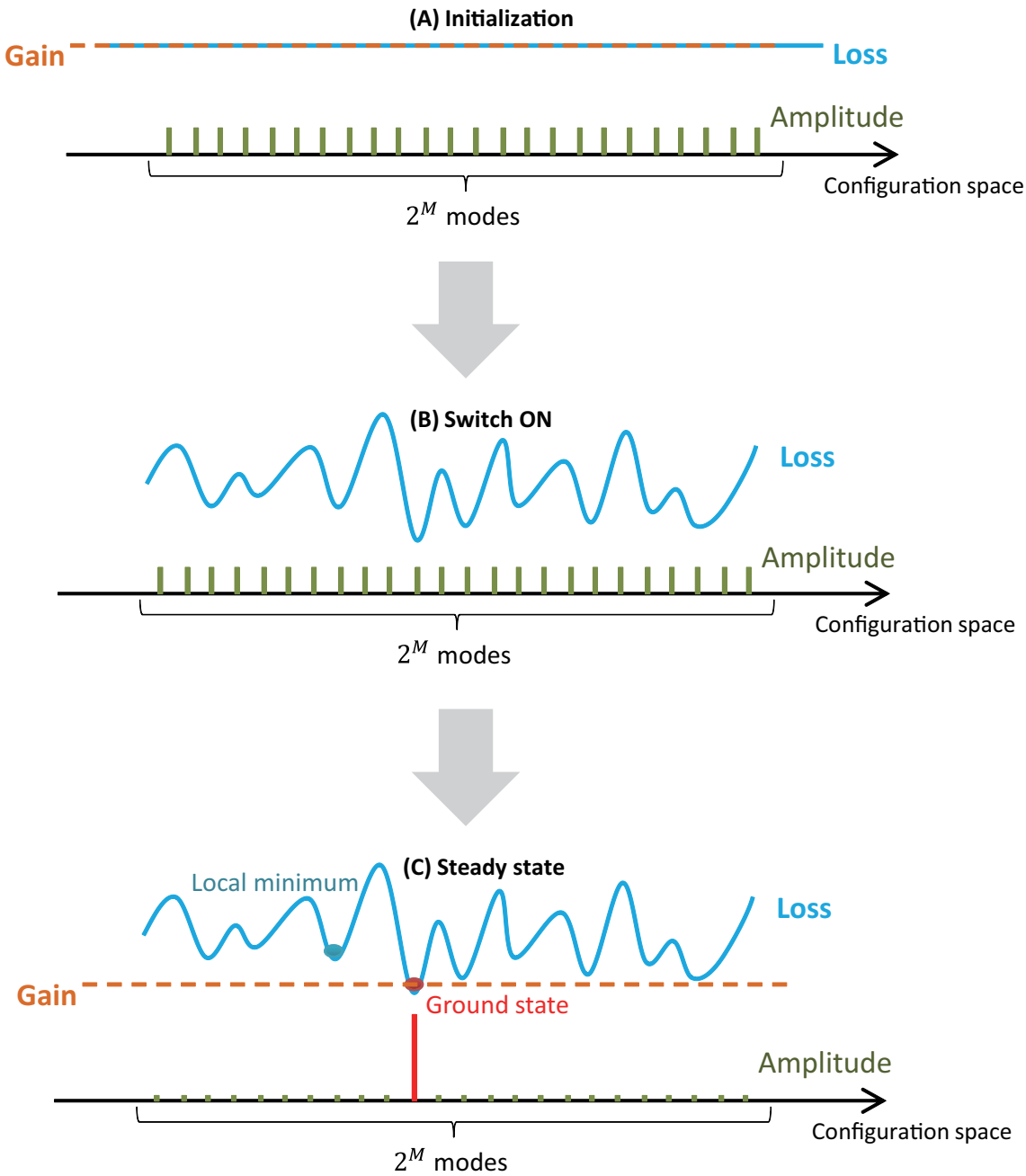

Figure 3.10: (A) The initial state at loss landscape for every mode configuration before the computation starts. (B) As the computation is switched ON, the loss landscape is implemented with the landscape of Ising energy of the specific problem. (C) As the system reaches to a steady state, only the ground state polarization configuration can exist. All the other excited configurations will decay exponentially. The dashed orange line is the gain which is equal to the loss at steady state. The vertical bars at the bottom are the amplitude of each mode, in which the red bar is the amplitude of the ground state for the Ising Hamiltonian.

loss landscape. In classical computation, such as simulated annealing and genetic algorithms, these local minima may trap the algorithm for very long time. Therefore the metastable states make it very difficult to find the correct global minimum. Unlike the local search algorithms, the laser network uses a different mechanism to find the mode in which the loss is minimized. Because the laser network is prepared in the coherent superposition of 2^M modes, it is able to probe the loss landscape for every mode simultaneously. Particularly, the gain in the laser system is saturated to the value equal to the loss by nonlinear effect, and the laser network should only have one total gain. First, the modes with loss higher than the saturated gain can not be supported by the laser network, and the populations on these modes are experience an exponential decrease given by the finite loss difference to the gain. Second, the only possible value the saturated gain may stay at steady state is the mode with the minimum loss. Otherwise, the mode with the minimum loss will have the gain greater than the loss and its population will still grow exponentially and violate the steady state condition.

The above two points lead to the minimum gain principle: at steady state the total gain is saturated to the minimum loss and only the mode with minimum loss can oscillate. We call it the minimum gain principle rather than the minimum loss principle, since the gain is also minimized when it get saturated. Driven by the minimum gain principle, the population on any mode corresponding to the excited state of an Ising model is dissipated to reservoir exponentially fast since there is finite loss difference, while the population on the mode corresponding to the ground state grows exponentially fast until saturated. At steady state, Figure 3.10 (C) show that

the gain is pinned to the minimum loss and only the corresponding mode is oscillating as shown at the bottom.

The minimum gain principle is different from the local search and it is free from the bottleneck of local minima. All possible mode configurations in the injection-locked laser network are evolving at the same time. Any mode with loss higher than the minimum loss will suffer from exponential decay even for metastable modes. However, as we will discuss in the next chapter, the injection-locked laser network has its own bottleneck which may generate an incorrect loss landscape and result in wrong answers.

3.6 Numerical simulation results

In this section we perform a series of numerical simulations using the photon number model and amplitutde and phase model respectively. The numerical simulation is using the fourth-order Runge-Kutta (RK4) method.

The site number M is varied from $M = 2$ to $M = 10$ for photon number model, where the Ising model parameters λ_i and J_{ij} are chosen so that the given Ising model has local minima separated from the ground state by a macroscopic Hamming distance (number of different spins between two spin configurations). Correct ground state configuration is obtained for the parameters J_{ij}, λ_i used for each M. These numerical simulation results are shown in Figure 3.11.

Figures 3.12 show the average amplitudes and phase in the two diagonal polarization modes for the three $M = 3$ problem, calculated by the amplitude and phase model. As expected from the picture shown in Figure 3.12, $A_{Di} = A_{\bar{D}i}$ is satisfied at

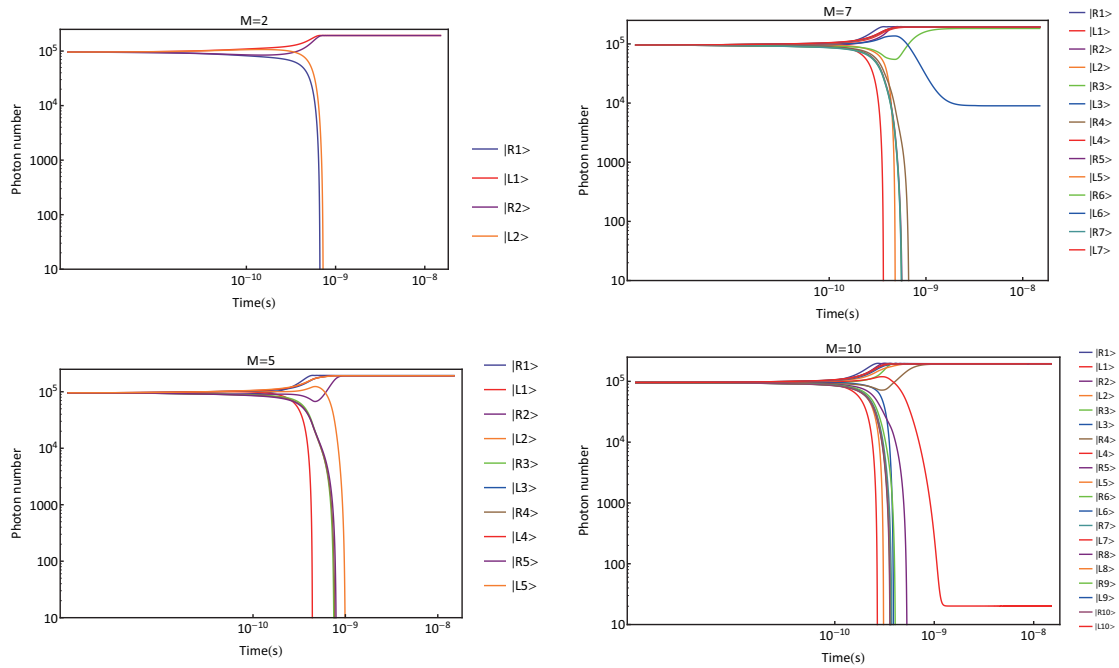

Figure 3.11: The time evolution of varied systems with site number from $M = 2$ to $M = 10$. We can find that the transient time does not depend on the number of sites. The time step is fixed at $\Delta t = 10^{-13}$sec, which is sufficiently short compared to any time constants appearing in. Since we neglect the quantum noise terms in the quantum mechanical rate equations, the numerical results shown in this section are for the ensemble averaged quantities.

all time, while ϕ_{Di} and $\phi_{\bar{D}i}$ depart with each other in a time scale shorter than 1 nsec and this phase modulation reaches the steady state within a few nsec. The slight and simultaneous increase in the amplitudes A_{Di} and $A_{\bar{D}i}$ results from the overall reduction in the photon loss rate.

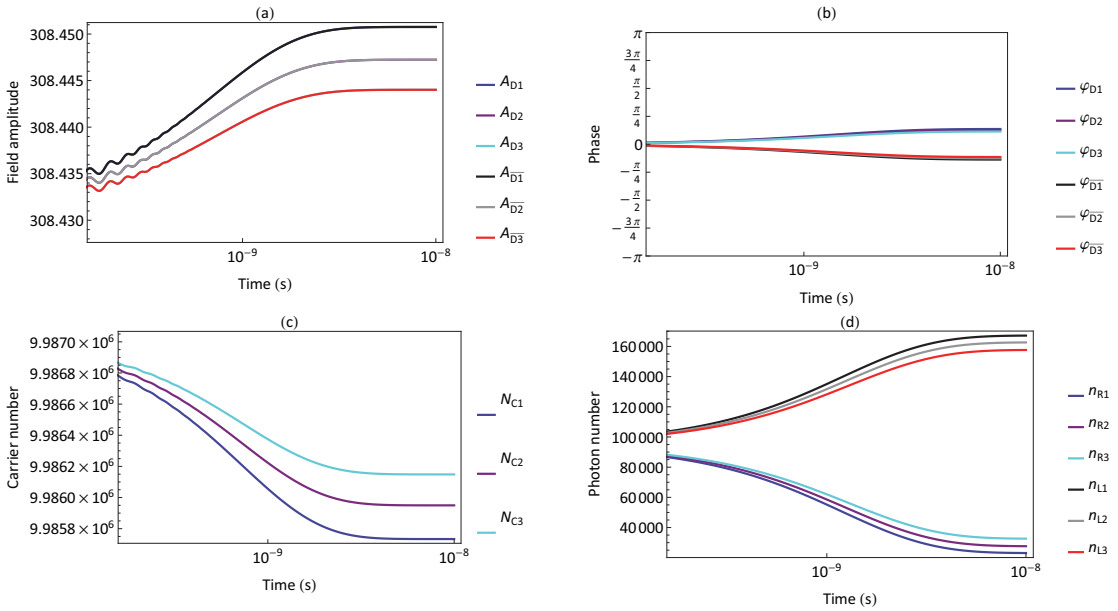

Figure 3.12: Averaged time evolution using amplitude and phase model for a laser network with 3 slave lasers.

Chapter 4

Solving NP-complete Problems using Coherent Ising Machine

In the precede chapters we introduced the architecture and basic behaviors of the coherent Ising machine. The systems implements an Ising model and finds its ground state according to minimal gain principle. In this chapter we look into the practical use of the proposed systems, in this thesis we focus on solving the representative NP-complete problem: 3SAT. First, we start from introducing the overall computation process and explain the function of each part. Second, we transform a simple 3SAT problem to Ising model using the method shown in Chapter 2. We will see that a feedback loop is applied to artificially generate the 3-spin interactions required in the transformation method. Third, we propose an algorithm that determines the optimal pumping power, which drive the system into just above the oscillation threshold. Fourth, the difficulties in solving practical problems such as frustrated spin and symmetry in Ising model is pointed out, to which we provide a simple approaches to

improve the success rate. Finally, we will reach to the conclusion of the computation time complexity of the coherent Ising machine from the benchmark simulation results.

4.1 Overall computation process

Solving 3SAT problems using the injection-locked laser network is consisted of repeating several stages. The overall cycle is shown in Figure 4.1. The pumping trial stage aims to find the optimal pumping rate for a specific problem setting. To determine the optimal pumping rate it requires multiple times of trial run for a certain time, each trial i uses a different candidate pumping rate P_i which is given by a binary search algorithm. Inside each trial run, there are multiple cycles of repeating the measurement process by photon detection, and then generating a Zeeman field according to the measurement result. The feedback Zeeman field is generated to artificially realize a 3-body interactions in the Hamiltonian of a 3SAT problem. The dynamic weight Zeeman field is generated to solve frustrated spin situations by put different weight on each 3SAT clause based on their current satisfiability. It is effective for a 3SAT problem with a large number of clauses. In each measurement, the spin configuration is observed in real-time by the photon detectors placed in each slave laser. The spin configuration is immediately sent to a verification circuit, where the current spin configuration is input to the 3SAT problem and the satisfiability is verified. The overall process is repeated until a satisfiable spin configuration is observed. In next sections we explain each stage in detail.

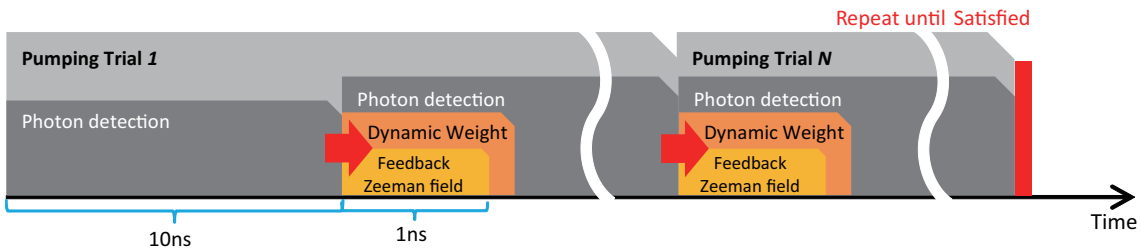

Figure 4.1: The overall computation process using the laser network to solve a 3SAT problem.

4.2 Artificial measurement and feedback loop

Giving a simple 3SAT problem with 3 variables and only one clause such as $(A + B + C)$, following the method given in Chapter 2 we create the correspondent Ising hamiltonian as

$$H = -a - b - c + ab + ac + bc - abc, \tag{4.1}$$

where a,b and c are Ising spins correspondent to the boolean variables A, B and C respectively. Since experimentally creating the three spin interaction term abc is a non-trivial task, the proposed Ising machine is extended with a measurement and feedback loop to virtually generate the 3-spin interaction term abc. In the injection-locked laser network we setup a photon detector into each slave laser site, to continuously detect the photon state inside the site (Figure 4.2). For the Hamiltonian (4.1), we denote the measurement result as $\langle a \rangle$, $\langle b \rangle$ and $\langle c \rangle$ respectively for each laser site correspondent to the Ising spin a, b and c. The measurement result is used to calculate the Zeeman field such as to generate the hamiltonian

$$H' = -a - b - c + ab + ac + bc - \frac{1}{3}(\langle b \rangle \langle b \rangle a + \langle a \rangle \langle c \rangle b + \langle a \rangle \langle b \rangle c), \tag{4.2}$$

where the $\langle a \rangle$, $\langle b \rangle$ and $\langle c \rangle$ take continuous value calculated by Eq. 3.46.

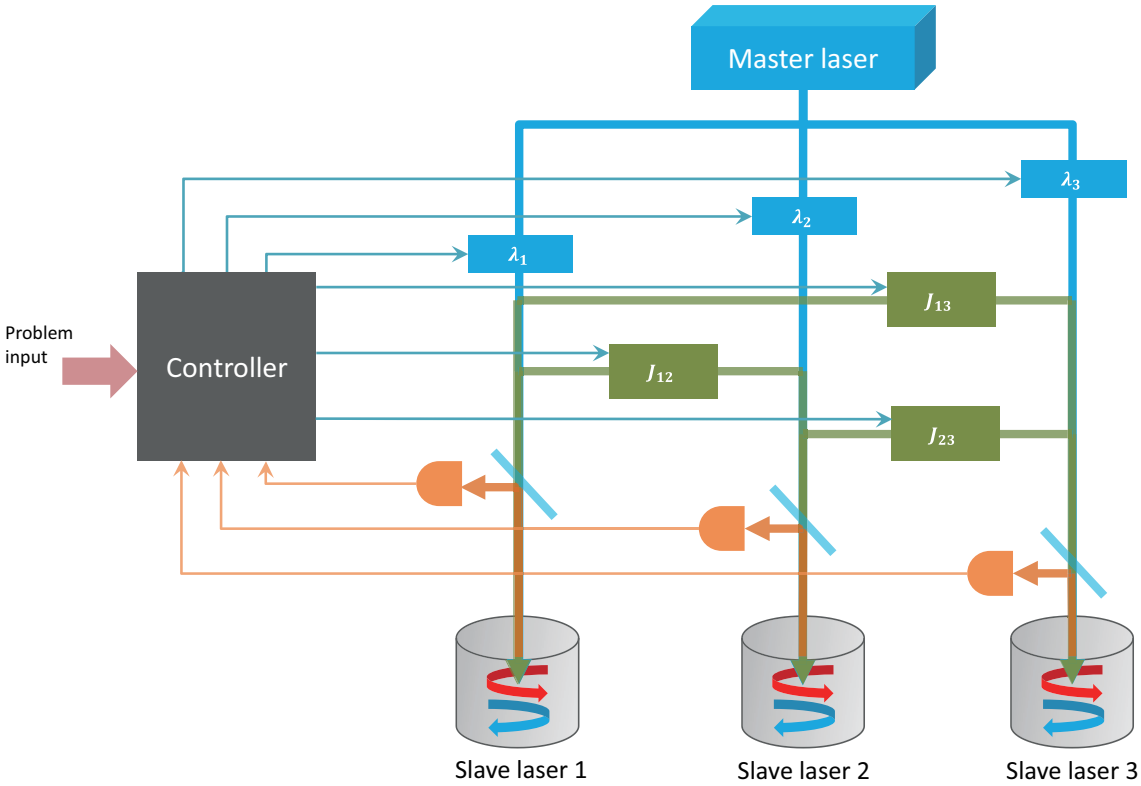

Figure 4.2: An Ising machine implemented using injection-locked laser networks is extended with a controller unit. The controller generates Zeeman fields to each site according to the detected states.

Compared to the response time of photons inside the laser site whose lifetime is ~ 1 ps, a photon detector usually takes several nano seconds to output a measurement result. Therefore the measurement and feedback loop is working in $\sim$ 100MHz update frequency as shown in Figure 4.3, which results in an approximated Hamiltonian with a certain amount of error due to outdated information. The controller unit is assumed to be implemented using electronic circuits such as FPGA [], for which to perform the 100MHz output frequency is a practical solution.

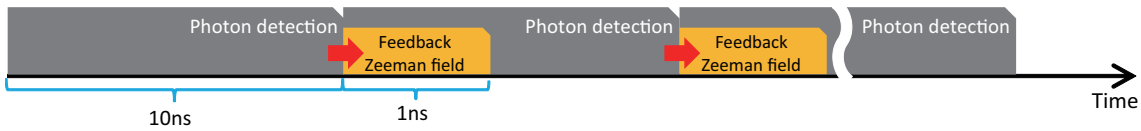

Figure 4.3: Photon detection and feedback process is repeated to artificially generate the 3-body interactions.

To validate the scheme (4.2), we compare the numerical simulation results of 3 settings. In Figure 4.4 there are three histograms. The ideal feedback is calculated by virtually exactly generating the Hamiltonian (4.1) by updating the measurement result and applying Zeeman field in infinite speed. It is compared with the delayed feedback loop for which the update frequency is slowed down to 100MHz, and the case in which the 3-spin interaction term is completely ignored is also simulated. From the result we can find that as feedback update frequency becomes slower, the system is more like to stay at the ground state of the approximated Hamiltonian whose 3-body interaction is ignored, rather than the ground state of the exact Hamiltonian (4.1).

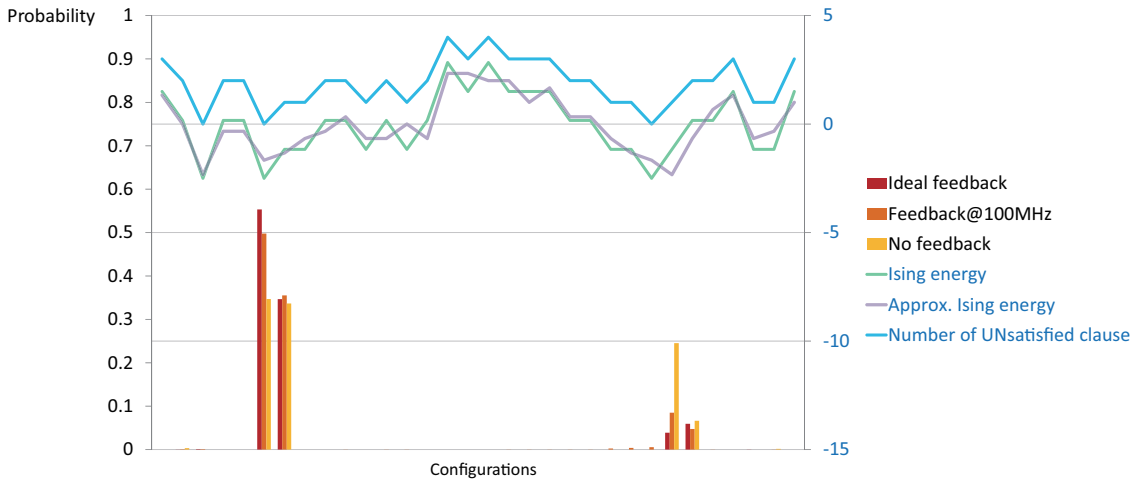

Figure 4.4: The energy landscape of a 3SAT problem with 5 sites and 20 clauses. The probability of systems to stay in a specific assignment is shown. Number of UNsatisfied clause equals to be 0 suggests a satisfying solution. Ensemble result from 100 trajectories. Ising energy is linearly scaled to fit within the plot area.

4.3 Optimal pumping power determination

As we see in the Chapter 3, the essential mechanism of the coherent Ising machine to find the ground state of an Ising model is the minimal gain principle. Under the optimal pumping power, when the system reaches at steady state, only the ground state configuration which correspond to the oscillation mode with minimal gain and loss can exist, and the amplitude of excited states will decay exponentially as shown in Figure 4.5 (A). However, If the pumping power is too high, there is a leakage to a large number of the first or even second excited states. For a hard problem instance, the number of the first excited states increases exponentially as the problem size. The ground state and excited states are separated by a macroscopic Hamming distance, so that the probability to transit local minimum and find the ground state will decrease significantly, as shown in Figure 4.5 (B). An actual example of the histogram of

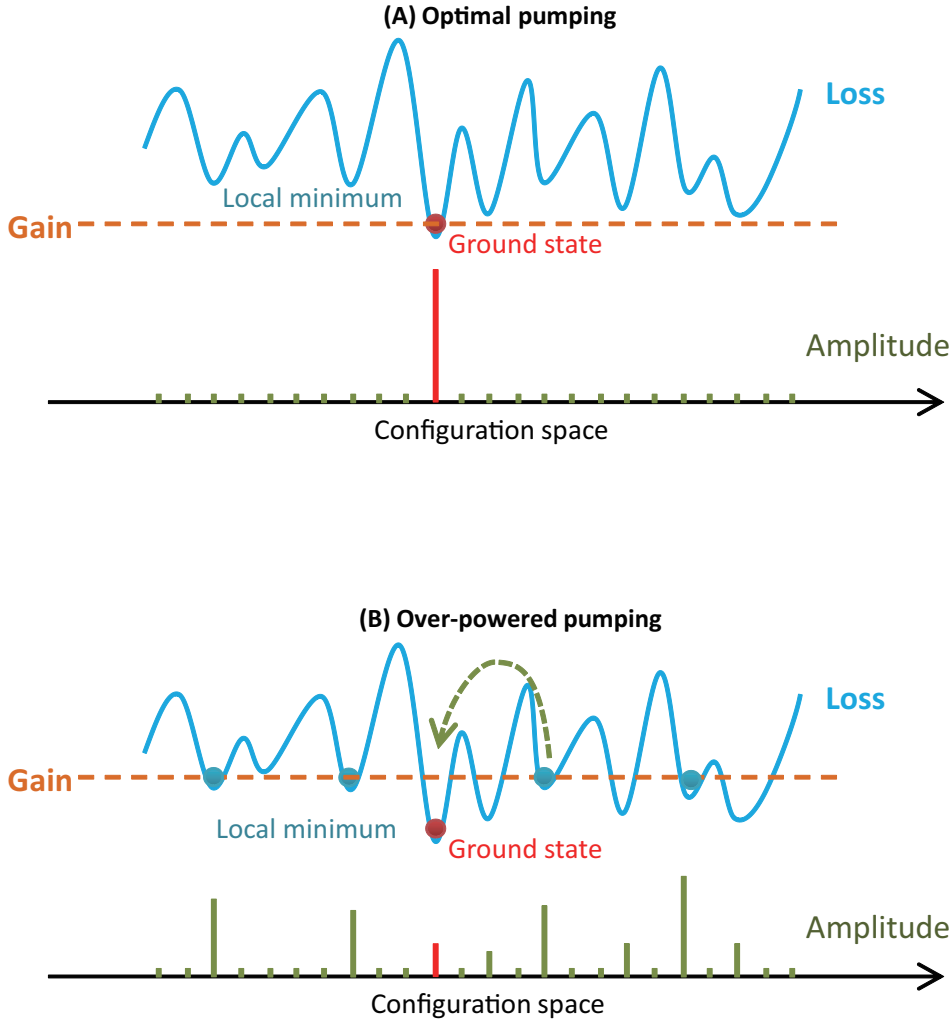

Figure 4.5: (A) When pumping rate is just above the overall oscillation threshold, the system will reach to a steady state where the gain for ground state mode is equivalent to the loss. (B) When pumping rate is too high, the system will stay at an equilibrium with excited states, in this case the system has to depend on random phase noise to find the ground state configuration.

solving a simple Ising model with different pumping rate is shown in Figure 4.6.

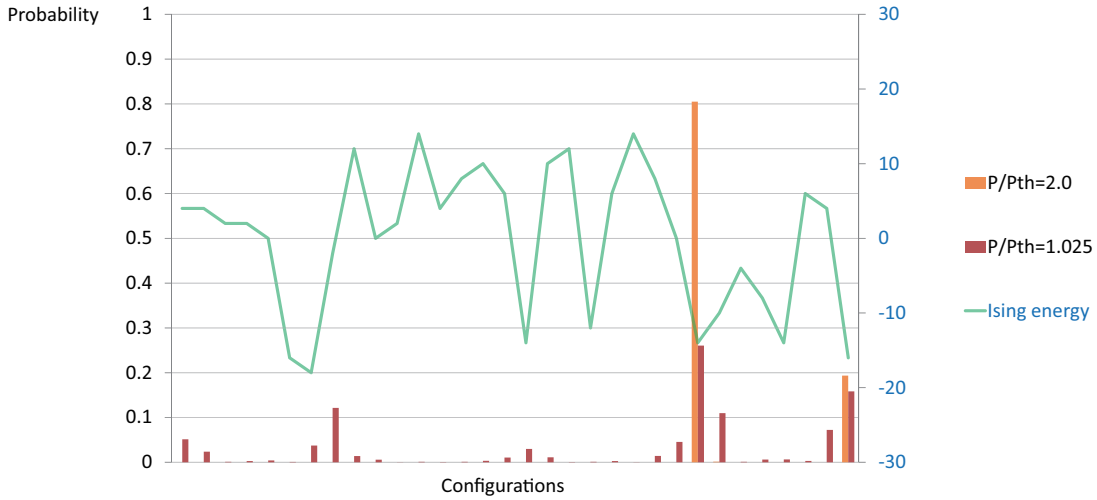

Figure 4.6: The system finds the ground state mode with reduced pumping power. The ground state is the one with Ising energy equal to 0.2 in the graph.

How to determine the optimal pumping rate which drive the system into just above the oscillation threshold is a problem. A simple strategy to remedy the problem would be gradually increase pumping rate. We fix the Zeeman term and mutual coupling first, then we slowly increase the pumping rate from well below the threshold to just above the threshold, The pumping should not increase to above the gain value at which any excited state can oscillate as shown in Figure 4.7 (A). As each time we change the pumping rate with a certain increased power, there is a transient time to wait and determine if the oscillation is generated after the change. If we increase the pumping power too fast before the system reaches the steady state, it is very possible to pass through the oscillation threshold and increase to the over-powered pumping rate. The procedure may take a long time, and the difference of pumping each time we change has to be controlled carefully.

To overcome the problem, we proposed another scheme using a binary search

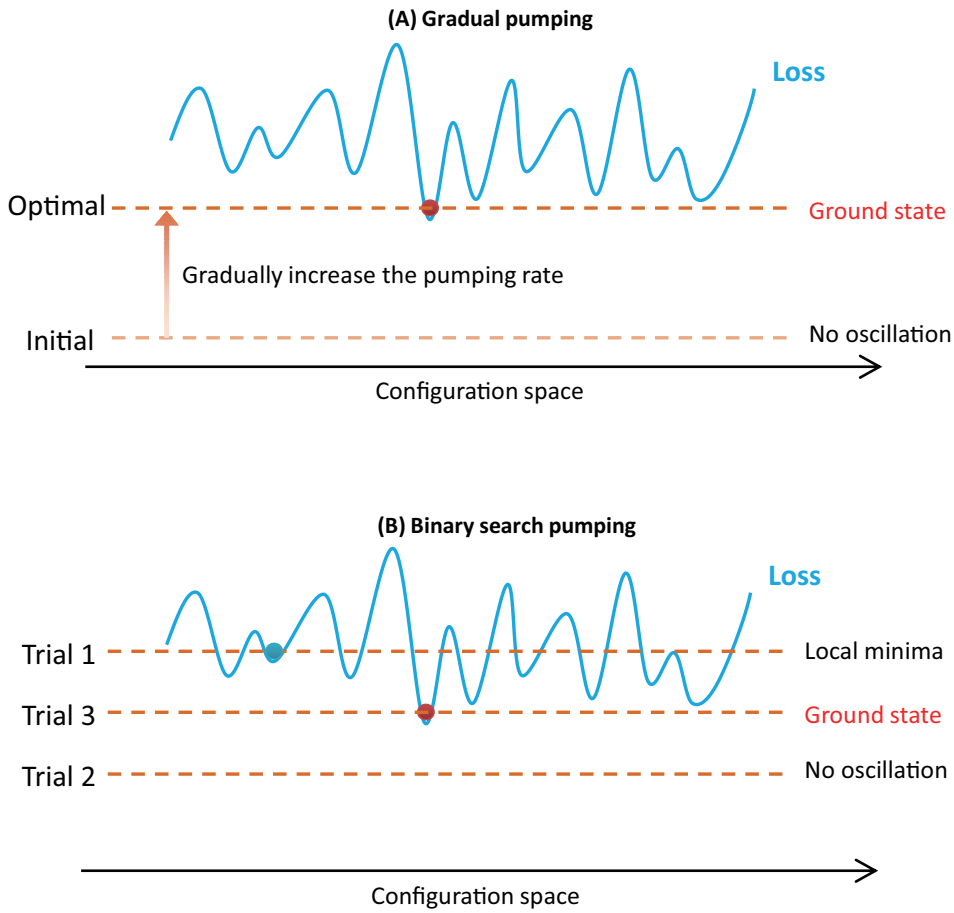

Figure 4.7: (A) Gradual pumping which starts from far below the oscillation threshold and gradually increase to find the optimal pumping rate. (B) Binary search the optimal pumping rate, which finds the threshold in several times of trial evolution.

method [] as shown in Figure 4.7 (B). Given a specific pumping rate, there are at most three cases: (a) Pumping rate is far below the oscillation threshold, which can not generate oscillation; (b) Pumping is just equal to the oscillation threshold, by which we can correctly find the ground state configuration; and (c) Pumping is too high above the oscillation threshold, by which we always reach to excited states. Therefore given the specific pumping rate, we can easily determine whether it is above or below the optimal pumping rate by a trial run for a certain time period long, and observe which is the result among the above cases. We choose a certain interval of search range with a lower limit P_{low} and a higher limit P_{high}. The initial P_{low} is set to a value where it is known that no oscillation can exist, we can simply set it to $P_{low} = 0$. On the other hand, the initial P_{high} is set to a value which is well above the threshold of the total system, for example $P_{high} = 2.0P_{th}$, where P_{th} is the pumping threshold pumping for the lasers without implementing the Hamiltonian (4.1). The actual pumping rate used in ith trial run is given by $P_i = \frac{1}{2}(P_{low} + P_{high})$. After each trial run we determine the next trial pumping rate according to the result. If the result is (a) then all values below P_i will be below the oscillation threshold, thus we update the lower limit of search interval to $P_{low} = P_i$. In contrast, if the result is (c) then all values higher than P_i will be over-powered and there will be less probability find ground state with those value, thus we update the higher limit of search interval to $P_{high} = P_i$. The next trial pumping rate is again decided by $P_{i+1} = \frac{1}{2}(P_{low} + P_{high})$ with the updated interval. Repeat this procedure until we find (b). The flowchart of the algorithm is depicted in Figure 4.8 and the computation cycle is shown in Figure 4.9.

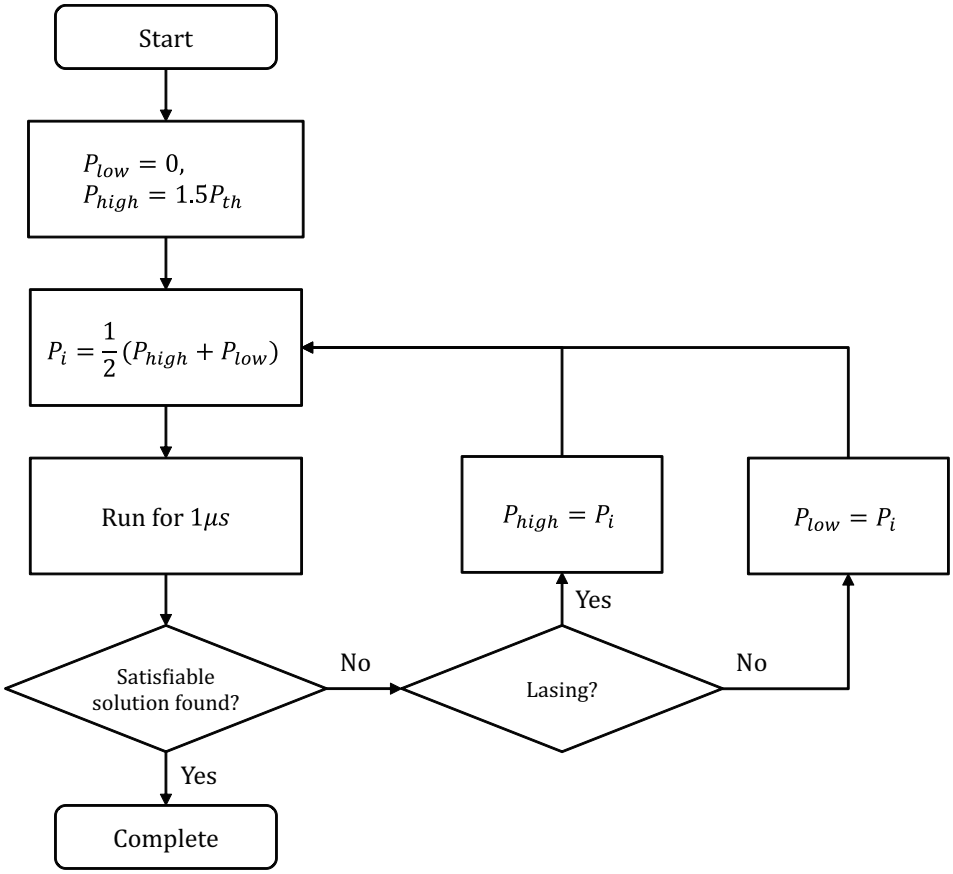

Figure 4.8: The flow chart of optimal pumping rate using binary search.

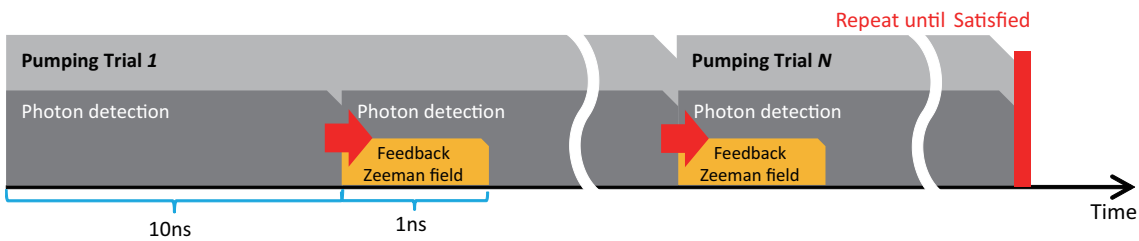

Figure 4.9: The computation process utilizing the optimal pumping rate determination.

Using the binary search method, each trial run will cut the search interval by half. As we will see later, a 3SAT problem with M clauses will generate M different energy level in the correspondent Ising Hamiltonian. Therefore the number required of repeating the trial process is within $O(logM)$.

Note here the condition (a) can be determined by observing the photon count after starting the trial run for a certain time, practically it can be set to $\sim 1\mu$sec which is sufficient long than the transient time and multiple times of feedback loops needed. If the photon count measured by the photon detectors at each slave laser is below a threshold number, for example $N_{threshold} = 1$, we can know the the pumping rate is not enough. Condition (c) can be determined by observing the result configuration at steady state. Since for a NP-complete problem such as 3SAT, given a specific spin configuration we can quickly if it is the optimal (Satisfiable) solution. If we always get wrong result from the measurement, we can determine that we are at far above the threshold gain. The binary search process will give the result either of (a) or (c) from each time of trial running, until we find the ground state in (b).

We simulated this process using varied 3SAT problems with $N = 5$ (number of variables) and $M = 45$ (number of clauses), the result is shown in Figure 4.10.

4.4 Dynamic weighted clauses

During the time evolution of the system, it is possible to meet an Ising interaction with contradictions. An intuitive example is illustrated in Figure 4.11, where for the specific spin i the signal comes from the coupled spins are suggesting an opposed value. Once the system meets such a situation, it is possibly to be trapped in the

Figure 4.10: Simulation of optimal pumping determination using 10 randomly generated 3SAT problem instances with $N = 5$ and $M = 20$. In all problems in the second trial using half the pumping rate of the initial value finds out the ground state. In problems with multiple ground states it is possible to detect different ground states with the lower pumping rate, while the initial higher pumping rate usually stays at only one ground state configuration.

situation.

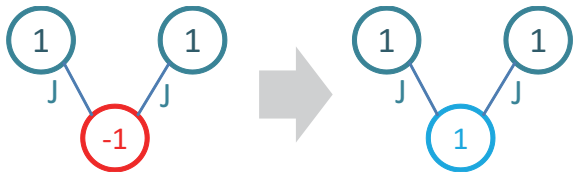

Figure 4.11: Wrong parity situation.

For 3SAT problems, these situations are considered to be originated from the symmetry of Hamiltonian (4.1), namely the disappearance of Zeeman terms. For example, given $(A + B + C)(\bar{A} + D + E)$, the partial Hamiltonian for the first and second clause are respectively

$$H_1 = -a - b - c + ab + ac + bc - abc, \tag{4.3}$$

$$H_2 = a - d - e - ad - ae + de + ade, \tag{4.4}$$

therefore the total Hamiltonian is

$$\begin{aligned} H &= H_1 + H_2 \\ &= -b - c - d - e + ab + ac - ad - ae + bc + de - abc + ade, \end{aligned} \tag{4.5}$$

where the Zeeman term for a is disappeared. Due to the lack of Zeeman field, the evolution of spin a is motivated only by Ising couplings. It is more probable to meet a frustrated or contradicted situation for a depend on the coupled spins. As the ratio of number of clauses and number of variables, namely M/N increases, the probability of generating the situations is raised up too.

A simple approach to avoid the problem is proposed by combine the partial Hamil-

tonians with a weighted coefficient, namely

$$H = c_1 H_1 + c_2 H_2, \tag{4.6}$$

where the coefficient for each clause c_i is simply decide by $c_i = C_{sat}$ if clause i is already satisfied using current spin configuration, otherwise $c_i = C_{unsat}$ if the clause is not satisfied yet. The ratio C_{sat} and C_{unsat} should be adjusted to $C_{unsat}/C_{sat} > 1.0$, however, not too much because a big difference between C_{sat} and C_{unsat} may cause a reverted bias thus to repeat the parity error situation in the opposite way, namely satisfied clauses and UNsatisfied clauses repeatedly change to each other. Experiences from numerical simulations for $N \sim 20$ instances have acquired an ideal ratio ~ 1.5. The satisfiability of each clause is also decided by the measurement and feedback circuitry used in applying the 3-body interactions. The effectiveness of the approach is shown in Figure 4.12. The computation process including the dynamic weighted clauses technique is shown in the above Figure 4.1.

Note that a self-learning technique is proposed to solve the similar situations in [39], which is based on artificially detecting and avoiding the frustrated spins and parity errors between the couplings. The technique is provided for solving NP-hard problems as well as NP-complete problems such as MAX-CUT problem. Since the essential cause of the situations are equivalent in 3SAT problems and MAX-CUT problems, therefore the solution is considered to be equally effective. The dynamic weighted clause directly use the information from 3SAT problem, thus it is acting on a macroscopic level compared to the self-learning method which utilize the information of each single spin and acts on a microscopic view. Since there are 3 variables in each clause in 3SAT problems, a weight coefficient c_i affect 3 spins at once in each

cycle, while the self-learning method affect a single spin in each step. Therefore there is considered to be several times of speed up for dynamic weighted clause than self-learning method.

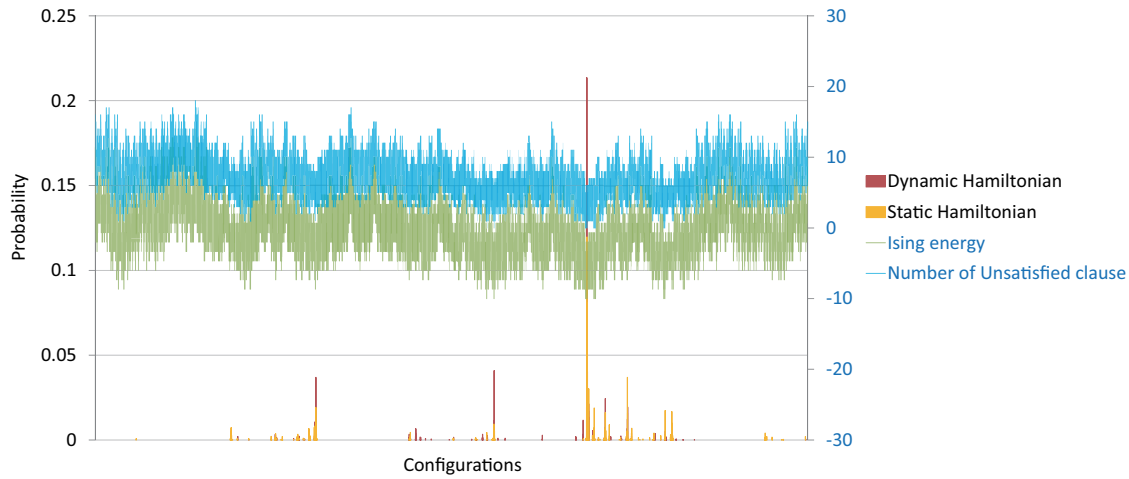

Figure 4.12: The dynamically weighted clause achieves a higher probability of staying at the correct ground states. The energy landscape histogram ensemble result from 100 trajectories.

4.5 Scaling of computation time with problem size

In this section we are interested in the scaling of computation time with input problem size. We solved 3SAT problems with different number of variables N. The number of clauses M is fixed to $M/N = 4$. Since there is a phase transition in 3SAT problems that the problem suddenly becomes intractably difficult when the ratio $M/N = 4.26$ [40], the $M/N = 4$ instances we used can be considered to among the most difficult instances in practical. The problem instances are generated using ToughSAT Random-k-SAT generator [41], which intentionally generates hard instances. In each pumping trial, the system is evolved for 10 nano seconds. Each

problem instance is evolved until a satisfied spin configuration is observed. The measurement and feedback loop is assumed to be ideal that is running in infinite speed. The result is shown in Figure 4.13. From the result we can see that both the total time which includes the pumping trials, and the satisfied time which is the time taken under the optimal pumping rate, are confined less than the exponential order. The approximated curve shows a $\sim O(N^3)$ time complexity, which is identical to the result acquired in [39] which uses MAX-CUT problems and approximated results.

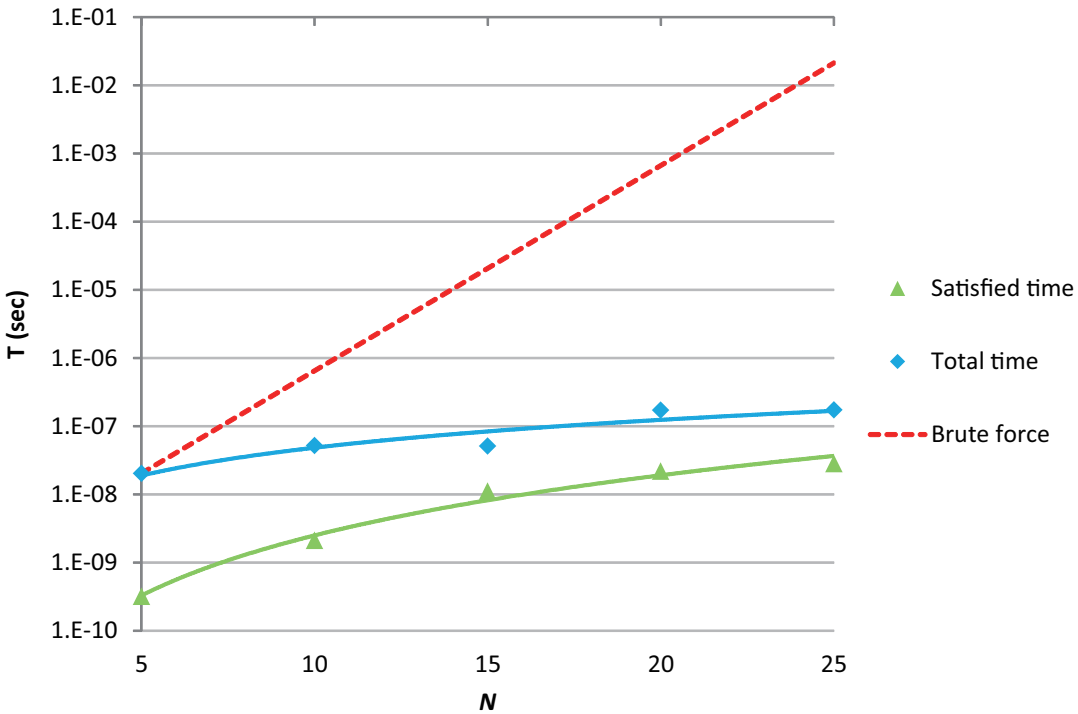

Figure 4.13: The computation time scale with the input problem size. 10 different 3SAT problem instances are generated for each N with $M/N = 4$. Averaged time is taken from 100 trajectories. The time needed to observe a satisfiable solution under optimal pumping power is the Satisfied time. Total time is the satisfied time added with number of failed trials multiple the running time period for the trial (10nsec).

Chapter 5

Conclusions and Outlooks

In this thesis we introduced the coherent Ising machine, which is a new scheme to solve optimization problems. A coherent Ising machine is an open system in comparison to the closed system of gate model quantum computer. The Ising model has the capacity to encode a NP-complete problem, thus provide the proposed system a much wider range of applications compared to unitary transformation model of quantum gate model.

The coherent Ising machine implemented using a injection-locked laser network is explained. The laser network is constructed using one master laser and N slave lasers. The slave lasers are injection-locekd by the master laser signal and to keep the coherency all over the network. The Zeeman terms are implemented by injection from the master laser to each slave laser, and the Ising coupling terms are implemented by mutual injection between slave lasers. The theoretical model reveals that by finding the minimum gain and loss of all possible modes, the laser network subsequently obtains the ground state of the Ising Hamiltonian. The minimum gain principle plays

a key role in the optimization process performed by the laser network. The intrinsic quantum noise of the lasers drives the system from the initial vertically polarized state to the final state in either right or left circular polarization where the total loss is minimized and the gain is saturated to the minimum loss. Otherwise, if the system stays in a mode with higher loss at steady state, the gain is saturated to the higher loss, and the population of the mode with the minimum loss will continue growing exponentially due to the finite difference between the gain and the minimum loss.

To investigate the ability of solving NP-complete problems using the coherent Ising machine, we start from the representative NP-complete class problem, 3SAT. Reducing a 3SAT problem with N variables and M clauses to an Ising model requires at least $2(N+M)$ sites, although it is a linear transformation, when the problem size becomes larger it will be a huge number of laser sites which brings in nontrivial difficulties to the physical implementation. We proposed a new way of mapping a 3SAT problem into an Ising model which only requires N sites. The proposed method generates an Ising model with an extension term that contains three spin couplings, to implement this term we use an artificial feedback loop in the laser network implementation. The feedback method will introduce a certain degree of error to the energy landscape of the original Hamiltonian. However, from the simulation results we find that even the three spin term is completely ignored, the decrease in success probability is limited due to the character of the system that is driven by the quantum phase noise.

In the laser network, if the pumping power is higher above the overall threshold, the system will potentially fall into a false local minimum in the energy landscape.

The very pumping power correspondent to the global ground state is unknown prior to the computation. To overcome such a crucial obstacle, we proposed a Binary search method in determine the optimal pumping rate. The general scheme starts the pumping power by an arbitrary pumping rate much higher above the lasing threshold, and adjust the pumping rate half the previous power up or down each time depending on whether the system is in a excited state where gives false answer or is below the lasing threshold. By repeating the process finally we reach the exact point of the optimal pumping power which gives the highest probability of finding the global ground state. To detect whether the system is in lasing mode or in excited state, we observe the photon number difference in two polarization modes. Given an energy landscape which contains $O(M)$ different energy levels, using the binary search we only need $O(logM)$ times to repeat the search process. The method provides a significant speed up to the original design of the proposed Ising machine.

We generated various of 3SAT problems with number of clauses to number of variables ratio $M/N = 4$, which are considered to be among the most difficult instance in 3SAT problems. The computation time to find the satisfiable solution to the problems is acquired using the numerical simulations. From the result we find the computation time does not scales exponentially with the increasing of problem size. Instead, it shows a $O(N^3)$ behavior in the time complexity. Since there are $5N$ equations for a system with N sites, the numerical computation does not scale exponentially with the increase of problem size. It is possible that the step size of integral calculations used in simulating the system has to be reduced, otherwise the calculation will diverge. This question is left for future investigation.

Bibliography

[1] M. R. Garey and D. S. Johnson. *Theoretical Computer Science*, 1:237–267, 1976.

[2] M. A. Nielsen and I. L. Chuang. *Quantum computation and quantum information.* Cambridge University Press, 2000.

[3] L. K. Grover. *Proceeding of the 28th Annual ACM Symposium of the Theory of Computing*, page 212, 1996.

[4] P. W. Shor. *SIAM J. Sci. Statist. Comput.*, 26:1484, 1997.

[5] M. R. Garey and D. S. Johnson. *Computers And Intractability.* W.H.FREEMAN AND COMPANY New York, 1979.

[6] V. Dotsenko. *Introduction to the Replica Theory of Disordered Statistical Systems.* Cambridge University Press, 2000.

[7] H. Nishimori. *Statistical Physics of Spin Glasses and Information Processing: An Introduction.* Oxford University Press, 2001.

[8] K. Binder and A. A. Young. Spin glasses: experimental facts, theoretical concepts, and open questions. *Rev. Mod. Phys.*, 58:801–976, 1986.

[9] A. Das and B. K. Chakrabarti. Colloquium: quantum annealing and analog quantum computation. *Rev. Mod. Phys.*, 80:1061–1081, 2008.

[10] M. Mezard, G. Parisi, and M. A. Virasoro. *Spin Glass Theory and Beyond.* World Scientific, 1987.

[11] B. K. Chakrabarti P. Ray and A. Chakrabarti. Sherrington kirkpatrick model in a transverse field: absence of replica symmetry breaking due to quantum fluctuations. *Phys. Rev. B*, 39:11828–11832, 1989.

[12] C. Carvalho B. Appoloni and D. de Falco. Quantum stochastic optimization. *Stochastic Proc. Appl.*, 33:233–244, 1989.

[13] G. E. Santoro R. Martonak and E. Tosatti. Quantum annealing by the path-integral monte carlo method: the two-dimensional random ising model. *Phys. Rev. B*, 66:094203, 2002.

[14] R. Martonak E. Tosatti G. E. Santoro and R. Car. Theory of quantum annealing of an ising spin glass. *Science*, 295(5564):2427–2430, 2002.

[15] R. D. Somma and C. D. Batista. Quantum approach to classical statistical mechanics. *Phys. Rev. Lett.*, 99:030603, 2007.

[16] T. F. Rosenbau J. Brooke, D. Bitko and G. Aeppli. Quantum annealing of a disordered magnet. *Science*, 284(5415):779–781, 1999.

[17] G. Aeppli and T. F. Rosenbaum. *Quantum Annealing and Related Optimization Methods.* Springer Verlag, 2005.

[18] T. Hogg M. Steffen, W. van Dam, G. Breyta, and I. Chuang. Experimental implementation of an adiabatic quantum optimization algorithm. *Phys. Rev. Lett.*, 90:067903, 2003.

[19] K. Yan T. Byrnes and Y. Yamamoto. Optimization using bose-einstein condensation and measurement feedback circuits. *New journal of Physics.*

[20] T. Byrnes K. Yan and Y. Yamamoto. Kinetic monte carlo study of accelerated optimization problem search using bose-einstein condensates. *Prog. Inform.*, 8:1–9, 2011.

[21] K. Takata S. Utsunomiya and Y. Yamamoto. Mapping of ising models onto injection-locked laser systems. *Opt. Express*, 19(19):18091–18108, Sep 2011.

[22] S. Utsunomiya K. Takata and Y. Yamamoto. Transient time of an ising machine based on injection-locked laser network. *New Journal of Physics*, 14(1):013052, 2012.

[23] C. E. Leiserson T. H. Cormen and R. L. Rivest. *Introduction to Algorithms.* MIT Press, 1990.

[24] S. A. Cook. The complexity of theorem proving procedures. *Proceedings of Third Annual ACM Symposium on the Theory of Computing*, pages 151–158, 1971.

[25] R. M. Karp. Reducibility among combinatorial problems. *Complexity of Computer Computations.*

[26] J. E. Hopcroft A. V. Aho and J. D. Ullman. *The Design and Analysis of Computer Algorithms.* Addison-Wesley, 1974.

[27] E. Ising. Beitrag zur theorie des ferromagnetismus. *Z. Phys.*, 31:253–258, 1925.

[28] M. J unger F. Barahona, M. Gr otschel and G. Reinelt. An application of combinatorial optimization to statistical physics and circuit layout design. *Operations research*, 36(3):493–513, 1988.

[29] M. O. Scully M. Surgent and W. E. Lamb. *Laser Physics*. Westview Press, 1978.

[30] H. Haug. Quantum-mechanical rate equations for semiconductor lasers. *Phys. Rev.*, 184:338–348, Aug 1969.

[31] G. Björk L. Gillner and Y. Yamamoto. Quantum noise properties of an injection-locked laser oscillator with pump-noise suppression and squeezed injection. *Phys. Rev. A*, 41:5053–5065, May 1990.

[32] R. J. Glauber. Coherent and incoherent states of the radiation field. *Phys. Rev.*, 131:2766–2788, Sep 1963.

[33] C. W. Gardinen and P. Zoller. *Quantum Noise*. Springer-Verlag, 2000.

[34] S. Machida Y. Yamamoto and G. Björk. Microcavity semiconductor laser with enhanced spontaneous emission.

[35] S. Kobayashi and T. Kimura. Injection locking in algaas semiconductor laser. *IEEE J. Quantum Electron.*, 17(5):681–689, 1981.

[36] Y. Yamamoto S. Kobayashi and T. Kimura. Optical fm signal amplification and fm noise reduction in an injection locked algaas semiconductor laser. *Electron. Lett.*, 17(22):849–851, 1981.

[37] H. A. Haus and Y. Yamamoto. Quantum noise of an injection-locked laser oscillator. *Phys. Rev. A*, 29:1261–1274, 1984.

[38] J. M. Radcliffe. Some properties of coherent spin states. *J. Phys. A: General Physics*, 4:313, 1971.

[39] S. Utsunomiya K. Wen, K. Takata and Y. Yamamoto. Self-learning injection-locked laser network for solving np-complete ising problems. In preparation.

[40] Peter Cheeseman, Bob Kanefsky, and William M. Taylor. Where the really hard problems are. *Proc. IJCAI-91*, pages 331–337, 1991.

[41] Henry Yuen and Joseph Bebel. Tough sat project, 2011.